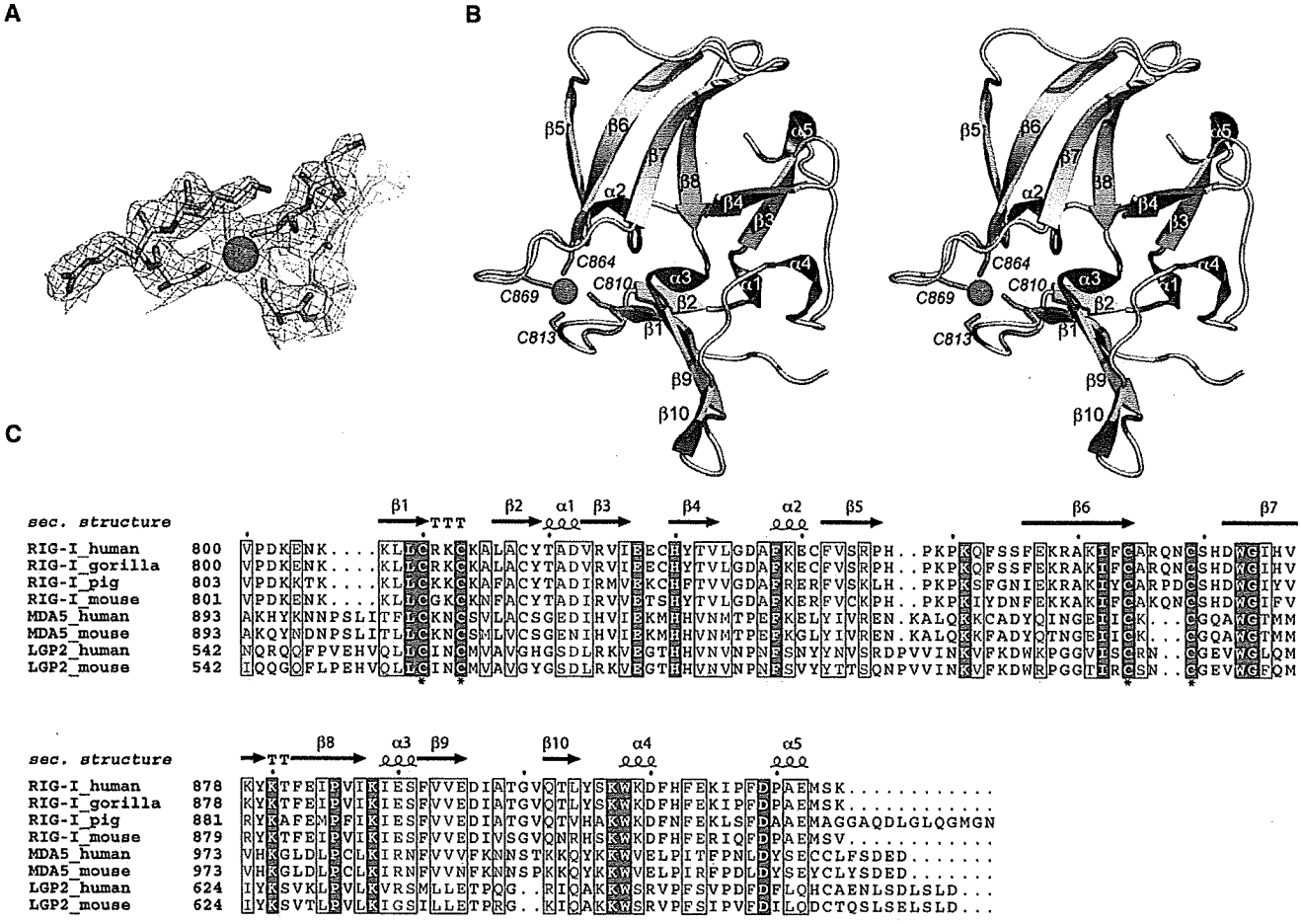

Figure 4. Structure of the Regulatory Domain of Human RIG-I

(A) Portion of the final $2F_o - F_c$ electron density (1 s contour) at the zinc-binding site with superimposed final model.

(B) Stereo image of a ribbon model of RD with highlighted and annotated secondary structure, zinc ion (magenta sphere), and annotated zinc-coordinating cysteines (green sticks).

(C) Structure-based sequence alignment of the C-terminal regions of RIG-I, MDA5, and LGP2 from different species. The secondary structure is shown on top. Invariant residues among RIG-I, LGP2, and MDA5 are highlighted with red background; conserved residues are shown in red font. The zinc-coordinating cysteines are marked with an asterisk.

structure of RD crystallized in the presence of zinc by molecular replacement. Both mercury- and zinc-bound structures, as well as all ten copies in the asymmetric unit, are highly similar to each other.

RD is a flat domain with a concave and convex side and dimensions of 45 Å × 35 Å × 30 Å (Figure 4B). It is structurally organized in three leaves, consisting of two four-stranded (β1, β2, β9, β10, and β5, β6, β7, β8) and one two-stranded (β3, β4) antiparallel β sheets. Small helical turns connect the three β sheets. The two four-stranded β sheets are laterally connected by two protruding loops, each containing two highly conserved cysteine residues (Cys810, Cys813 and Cys864, Cys869). Together, the four thiol groups of these cysteines coordinate the zinc (or mercury) ion in each of the ten molecules in the asymmetric unit (Figures 4A and 4B).

The zinc-coordinating cysteines are invariant not only in all available RIG-I sequences but also in all available MDA5 and LGP2 sequences, suggesting that this motif is a central functional or structural element in the entire family. Sequence representatives are shown in Figure 4C. Apart from the zinc coordination site, several other residues that form the hydrophobic core or are involved in fold stabilization (F838, W873, P885, and W908) are conserved between RIG-I, MDA5, and LGP2. Because these residues are distributed across the RD sequence, the fold of RD is probably conserved between RIG-I, MDA5, and LGP2. One possibility is that RD domains in MDA5 and LGP2 could possess similar, ligand-dependent dimerization functions. We tested whether MDA5 RD can bind to pppRVL (Figure 2A) but did not see significant binding. Thus, either different types of ligands are recognized by "RD" of MDA5, or this domain has a different functional role. For instance, the RD of MDA5 could be involved in detection of RNA elements that resemble poly(I:C), a known activator of MDA5. At present, we could not analyze the RD of LGP2 because of protein instability.

Table 1. Crystallographic Data and Model Statistics

	Hg-Acetate		Native (Zinc)
Data Collection	Inflection	Peak	
Space group	$P2_1$	$P2_1$	$P2_1$
Cell dimensions			
a, b, c (Å)	a = 97.20	a = 97.15	a = 97.9
	b = 76.60	b = 76.54	b = 76.6
	c = 137.80	c = 137.90	c = 139.4
α, β, γ (°)	90, 93.1, 90	90, 93.07, 90	90, 93.3, 90
Wavelength	1.010	1.008	0.9
Resolution (Å)	3.2	2.7	3.0
R_{sym}	7.9 (52.1)[a]	6.7 (43.8)	9.0 (44.5)
I/σI	14.49 (2.58)	14.36 (3.04)	8.97 (2.13)
Completeness (%)	98.3 (94.6)	98.1 (94.4)	98.0 (98.0)
Redundancy	3.87	3.88	2.54
Refinement			
Resolution range (Å)	20–2.7		50–3.0
Number of reflections	48,855		40,897
R_{work}/R_{free}	24.1/27.6		24.8/28.5
Number of atoms			
Protein	9990		9990
Ligand/ion	10 mercury		10 zinc
Water	124		49
B factors			
Protein	51.62		48.66
Rmsd			
Bond lengths (Å)	0.007		0.008
Bond angles (°)	1.49		1.52
PDB accession code	2QFD		2QFB

[a] Highest resolution shell is shown in parentheses.

RIG-I RD Is Structurally Related to MSS4 GDP Exchange Factor of Rab GTPases

Our data from the in vitro ATPase experiments indicate that RD is not only important for 5′-triphosphate binding but also activates the DECH box domain. To learn more about the functional architecture of RD, we looked for structural relatives in the protein data bank (PDB) using the DALI search tool (Holm and Sander, 1993). We found two significant hits (Figure S4). RD is related to the C-terminal methionine sulfoxide reductase domain of PilB (PDB entry 1L1D), although this structure lacks the zinc-binding site. However, both fold and zinc-binding site of RD are related to MSS4, a GDP/GTP exchange factor for small Rab-like GTPases (PDB entry 2FU5) (Figure 5A).

The zinc knuckle protein MSS4 stimulates nucleotide exchange by structurally modulating the nucleotide-binding site of the Rab8 GTPase (Itzen et al., 2006). Hereby, the zinc-binding site and its adjacent β sheets form the main interaction site to Rab8 and are a central element of MSS4-induced local unfolding of Rab8. The capability to locally unfold a GTPase active site is perhaps in part achieved by the rigid, thermodynamically stable architecture of the zinc cluster (Yu and Schreiber, 1995).

The structural similarity in both fold and zinc cluster raises the possibility that RD activates RIG-I not only by binding to 5′-triphosphates and dimer formation but also by some sort of structural modulation of the ATP-binding site, similar to the role of MSS4 in the activation of Rab8. While such a role needs to be addressed in future studies, it predicts that the zinc coordination site is a key functional element of RIG-I activation by RD.

The Zinc-Binding Site Is Essential for RIG-I Function In Vivo

To test the functional relevance of the zinc-coordinating cysteine residues of RD in vivo, we analyzed full-length RIG-I mutants, where RD cysteines have been mutated to arginine (Figure 5C) or alanine (Figure S5). RIG-I RD contains seven cysteines (Figures 4C and 5B). C810, C813, C864, and C869 are conserved in RIG-I, MDA5, and LGP2 and form our identified zinc-binding site. C818, which is conserved between RIG-I and MDA5 but not LGP2, is located close to the zinc-binding site but does not bind the metal ion directly. Two additional cysteine residues (C829 and C841) in the RIG-I RD are conserved between species, but not in MDA5 and LGP2.

Wild-type and mutant RIG-I were tested for their ability to trigger IFN-β promoter activation in response to infection with VSV-M51R (Figure 5C). Overexpression of WT *RIG-I* confers a low level of constitutive IFN-β promoter activation in the absence of ligand (15-fold induction compared to vector control). Infection with VSV-M51R led to a strong induction of IFN-β promoter activity (32-fold compared to mock infected cells expressing WT *RIG-I*). Induction is also observed for *RIG-I* harboring C829R and C841R (nonconserved cysteine) mutations. However, mutation of any one of the four invariant cysteines that coordinated the zinc (C810, C813, C864, and C869) or C818 to arginine abrogated the response to VSV-M51R. These defects, with the exception of C818R, are not due to insufficient protein levels (Figure S6) or to a dominant-negative inhibition of endogenous RIG-I (Figures S5 and S7). Similar results were obtained with mutations of conserved cysteines to alanines (Figure S5) and also in a cell line lacking functional endogenous RIG-I (Huh7.5 [Sumpter et al., 2005]; Figure S5). Activation of the IFN-β promoter after transfection of higher amounts of expression plasmids suggested intact constitutive signaling of RIG-I invariant cysteine mutants (Figure 5C, insert). WT RIG-I was activated by total RNA isolated from VSV-infected cells and by in vitro-transcribed 5′-triphosphate VSV leader RNA (pppVSVL), whereas the RIG-I C→R (mutated in all invariant cysteines of RIG-I RD) did not respond to either of the specific RIG-I ligands tested (Figure 5D). However, similar to WT RIG-I the RIG-I C→R mutant was able to interact with IPS-1 in the absence of RIG-I ligands in cotransfection experiments, confirming integrity of the CARDs in the presence of mutations affecting structure and function of the RD (Figure S8).

Taken together, our data show that the zinc coordination site is a key structural motif of RIG-I in vivo. The strong effect of C818R, which does not coordinate zinc and is located in the hydrophobic core of RD, is likely due to the lack of detectable protein levels, perhaps induced by misfolding (Figure S6). C829 and C841, on the other hand, are located on the RD surface, and the remaining responsiveness of the corresponding mutants to RIG-I ligand argues that these residues are not involved in a critical functional site.

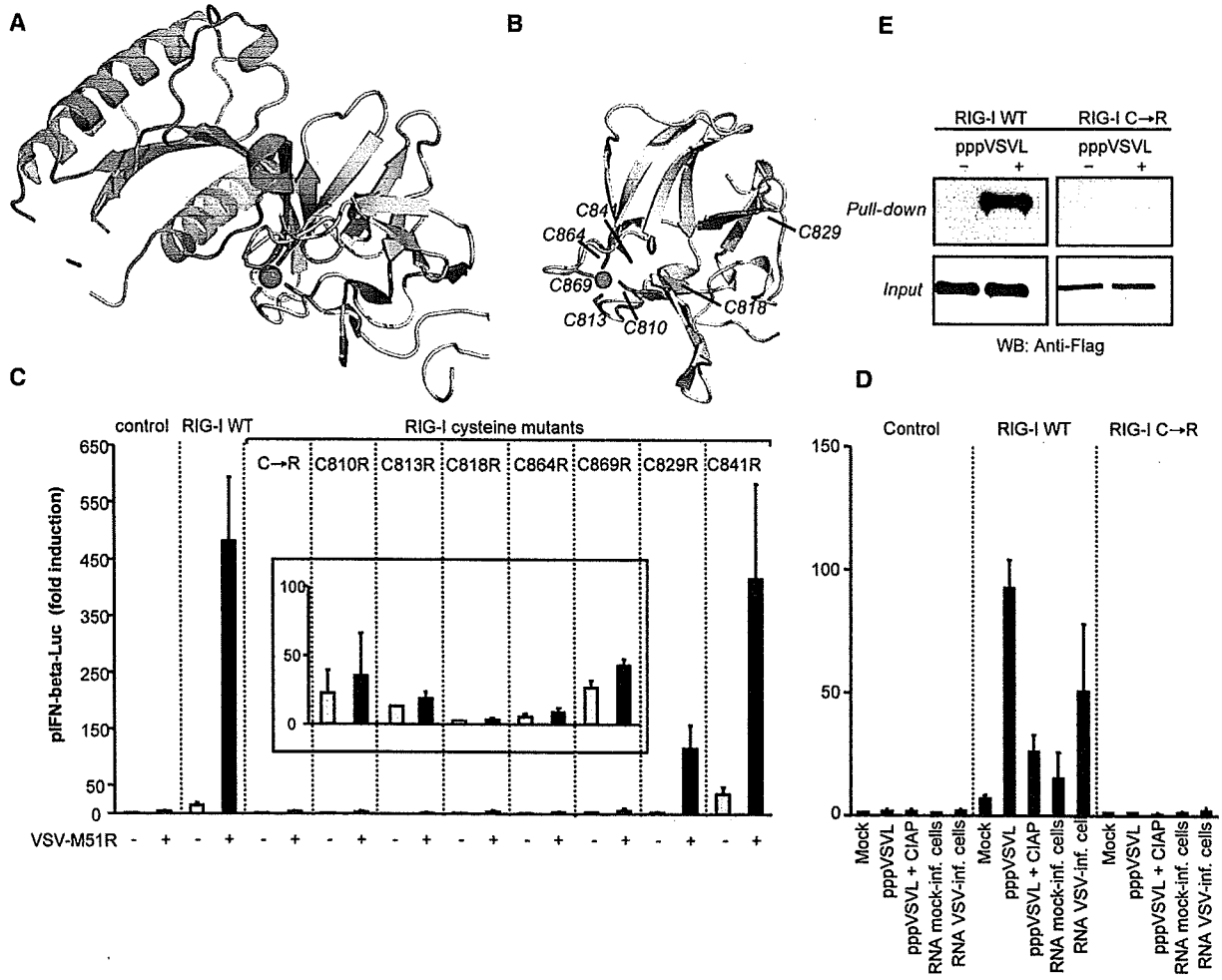

Figure 5. RIG-I Is Related to GDP/GTP Exchange Factors and Contains an Essential Zinc-Binding Site

(A) The fold and zinc-binding site of RD (shown in [B]) are related to GDP/GTP exchange factor MSS4 (yellow/brown ribbon model with green cysteines and magenta zinc). MSS4 induces GDP/GTP exchange in Rab8 (blue ribbon model) by local unfolding (Itzen et al., 2006).

(B) Location of cysteine residues (green sticks) on RD (gray ribbon model with magenta zinc ion).

(C and D) Conserved (C810, C813, C818, C864, C869) and nonconserved (C829, C841) cysteine residues in the RD of RIG-I were mutated to arginine. In the RIG-I C→R mutant, all five conserved cysteines were mutated to arginine. HEK293 cells were transfected with IFN-β promoter luciferase reporter constructs and renilla luciferase control vector as well as plasmids expressing WT RIG-I or RIG-I cysteine mutants using 100 ng or 400 ng per transfection (C, insert). Cells were subsequently stimulated (C) by infection with VSV-M51R and (D) in vitro-transcribed VSV leader RNA (pppVSVL ± dephosphorylation with CIAP) or RNA isolated from mock-infected and VSV-infected HepG2 cells. IFN-β promoter activity was measured by dual luciferase assay after 18 hr (fold induction compared to mock-treated empty vector control). Mean values and standard deviations of five (C) and four (D) independent experiments are shown.

(E) The cytoplasmic fraction of cells transfected with Flag-tagged WT RIG-I or RIG-I C→R mutant was incubated with biotinylated pppVSVL. RNA-protein complexes were pulled down using streptavidin affinity beads. Input and pull-down samples were analyzed by SDS-PAGE and immunoblotting using anti-Flag antibody (one representative of two experiments is shown).

Because RNA 5′-triphosphates appear to directly interact with RD in vitro, we tested whether the integrity of the zinc-binding site disrupts pppVSVL binding of RIG-I in vivo. Cytoplasmic extracts of cells transfected with WT *RIG-I* or the *RIG-I* C→R mutant were incubated with biotinylated pppVSVL and subjected to pull-down assay using streptavidin beads to recover RNA-protein complexes. pppVSVL was found to bind strongly to WT RIG-I, but not to mutant RIG-I (Figure 5E). Therefore, the integrity of the zinc-binding site of RD is essential for binding of pppVSVL by RIG-I in vivo and these data further corroborate our in vitro finding that RD is the RNA 5′-triphosphate sensor of RIG-I.

A Conserved Groove Is Involved in Binding of 5′-pppRVL

Our functional data show that RD does specifically recognize 5′-pppRVL, but not dephosphorylated RVL. Protein sites that bind triphosphates with high affinity, such as the active site of ATPases, often contain a positively charged patch to compensate the negative charge of the triphosphate chain, and the binding sites are often highly sequence conserved. We have not been able to cocrystallize RD with pppRVL or phosphates. To learn more about the potential triphosphate-binding site, we analyzed the sequence conservation and electrostatic potential at the solvent-accessible surface (Figures 6A and 6B). We find a highly

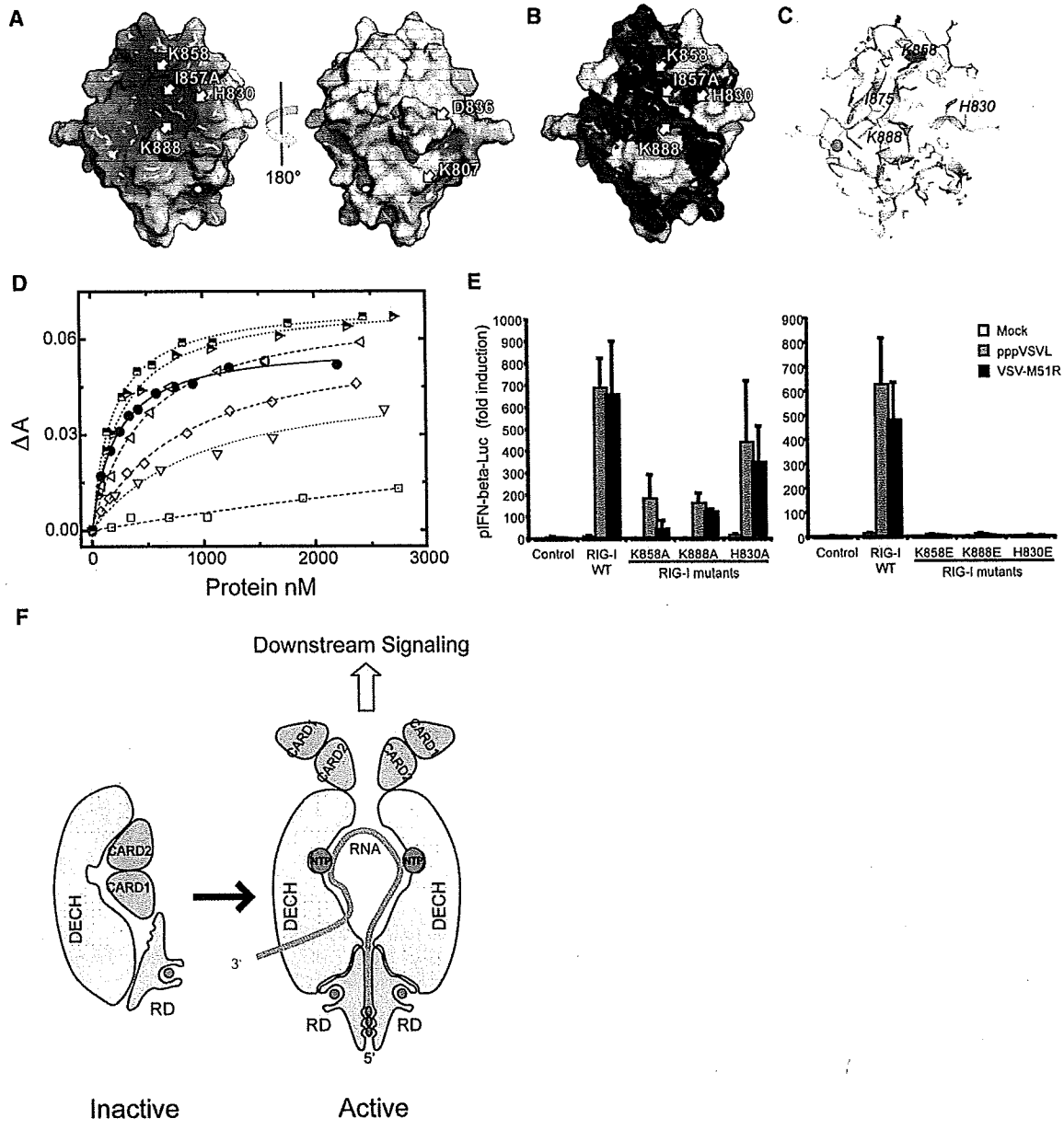

Figure 6. Localization of the RNA 5′-Triphosphate-Binding Site on RD

(A) Electrostatic surface potential (ranging from blue = 9 kT/e to red = −9 kT/e), displayed in two different views (left, "standard view" used in all other figures; right, 180° rotation around vertical axis). The sites of mutated residues are annotated. A prominent positive groove indicates a likely phosphate-binding site for RNA 5′-triphosphates.

(B) Surface conservation of RIG-I RD in standard view, ranging from dark red (invariant) to white (unconserved). A patch of high sequence conservation colocalizes with the positively charged groove (A, left).

(C) Localization of the mutations, shown in a ribbon model with added side chains. The effect of alanine mutations on pppRVL binding in vitro is highlighted by different colors: red, large effect; orange, medium effect.

(D) Fluorescence anisotropy changes (ΔA) of fluorescently labeled pppRVL in response to titration with WT RD (filled circle, K_d = 217 ± 11 nM) and mutated RD using the setup of Figure 2A. Two control mutations of conserved residues of the convex side of RD, K807→A (half-filled right-facing triangle, K_d = 254 ± 16 nM) and D836→A (half-filled square, K_d = 185 ± 15 nM), did not significantly alter binding affinity of pppRVL. Several mutations in the positively charged groove reduced binding affinity. H830→A (open left-facing triangle, K_d = 500 ± 30 nM), I875→A (open diamond, K_d = 1.0 ± 0.1 μM), and K888→A (open down-facing triangle, K_d = 1.0 ± 0.2 μM) significantly reduced binding affinity. K858→A (open square, K_d > 5 μM), however, dramatically reduced binding affinity, indicating that this residue is a central recognition site for pppRVL.

(E) HEK293 cells were transfected with IFN-β promoter luciferase reporter constructs and renilla luciferase control vector as well as plasmids expressing WT RIG-I or indicated mutants (10 and 100 ng per transfection). The left panel depicts the more conservative alanine mutants, while the right panel depicts the stronger glutamate charge reversal mutants. Cells were stimulated with transfected pppVSVL or infected with VSV-M51R. IFN-β promoter activity was measured by dual

positively charged groove at the concave side of RD that colocalizes with a region of high sequence conservation. To analyze this putative RNA 5′-triphosphate recognition site, we tested a variety of RD mutants in this region for interaction with pppRVL, using our fluorescence anisotropy assay (Figures 6C and 6D and Table S3).

Two control mutations (K807A and D836A), located on the convex side of RD, did not significantly alter the binding affinity for pppRVL, although these residues are highly sequence conserved. In contrast, three mutations in conserved residues inside the positively charged groove significantly reduced the binding affinity (H830A, I875A, and K888A). The mutation K858A, however, located at the center of the positive patch, dramatically reduced binding of pppRVL. This strong effect indicates that the groove is involved in the binding of the RNA 5′-triphosphate. We tested the K858A, K888A, and H830A mutants in vivo and found a significant reduction, but not complete abrogation of IFN-β promoter activity induced by transfection with pppVSVL or infection with VSV-M51R (Figure 6E, left). Mutations to negatively charged glutamates in the same positions (K858E, K888E, and H830E) entirely abrogated the response to pppVSVL and VSV-M51R (Figure 6E, right). The similar relative reductions in activity of the mutants in in vitro and in vivo experiments argue that the RNA binding defects observed in vitro are also the cause of reduced activity in vivo. Together, these observations suggest that interaction of VSV-RNA with the positively charged patch of the groove is required for full activation of RIG-I in vivo.

We do not see significant binding of fluorescently labeled UTP to RD (data not shown), which also contains a triphosphate. Thus, RD recognizes more than the triphosphate and sugar/base moiety of the 5′-terminal base of pppRNA. However, if RNA extends from K858 along the longest dimension of RD, the footprint will cover at most three bases, indicating that recognition of viral RNA by RD is limited to the very 5′-terminal region. This argues that adjacent 3′ regions could then bind to the RNA-binding sites of the DECH box domain.

Proposed Model for RD-Dependent RIG-I Activation

In summary, our data suggest a model for RIG-I activation that includes the following chain of events (Figure 6F). In the absence of 5′-triphosphate containing RNA ligands, RIG-I is monomeric and inactive. The CARDs probably partially mask an RNA-binding site on the DECH box domain. The preference of the DECH domain for dsRNA indicates that this RNA-binding site could also recognize secondary structures of virus RNA. pppRNA binding to RD induces a conformational change in the enzyme that results in dimerization and stimulation of the DECH box domain. The dimer form could, for instance, enable the binding of dsRNA or other types of RNA to the DECH domain by displacing the CARDs, and, in conjunction with or coupled to RNA-stimulated ATPase activity, this structural change might generate a signaling conformation of RIG-I. In analogy to adenosine triphosphate binding-dependent structural switches in many ATPases (Hopfner and Tainer, 2003), the binding energy of RNA 5′-triphosphates, which is likely in the same range as the binding energy of ATP to ATPases, is well suited to trigger such a macromolecular conformational change.

RIG-I RD mutants that have strongly reduced signaling activity are still able to interact with IPS-1 (Figure S8). We do not know at the moment how a RIG-I:IPS-1 interaction might lead to initiation of downstream signaling. Our dimerization results make it likely that the IPS-1:RIG-I signaling conformation includes a RIG-I dimer and for that reason possibly also an IPS-1 dimer. Because RD helps to stabilize an inactive conformation of CARDs (Saito et al., 2007), RD mutations might allow or even stimulate CARD exposure and thus IPS-1 interaction, but prevent pppRVL-induced RIG-I dimer formation and for that reason signal induction.

In conclusion, our data reveal the binding site for 5′-triphosphates on RIG-I, located on the C-terminal regulatory RD domain. At the center of this binding site is a RIG-I invariant lysine residue that is critically required for triphosphate binding. This lysine is partially buried, similar to the lysine in the P loop of NTPase, and this location is well suited for phosphate interaction. Interestingly, LGP2 contains a proline at the position of RIG-I K858, while MDA5 either contains a threonine or an isoleucine (Figure 4C). Consistent with this observation, we did not see strong binding of pppRVL to RDs of MDA5 and LGP2 (data not shown). Thus, RDs of MDA5 or LGP2 might either bind to different types of ligands or fulfill different functional roles. In any case, the RD of the three related DECH box ATPases could be an important specificity element. Thus, our results not only provide a structural framework to further analyze the specific recognition of viral RNA synthesis products by RIG-I, but could also to help to reveal the recognition of any ligands by the RDs of MDA5 or LGP2.

EXPERIMENTAL PROCEDURES

Protein Expression and Purification

RIG-I and MDA5 were expressed in insect cells as described previously (Berger et al., 2004). Briefly, cDNA was cloned into pFBDM vectors (MultiBac system, kindly provided by I. Berger) and transformed into DH10MultiBac cells. The bacmids were extracted for transfection into High-five insect cells (Invitrogen). Seventy-two hours after infection, the cells were harvested and lysed by "freeze and thaw." All other RIG-I and MDA5 constructs were expressed in *E. coli* BL21 Rosetta cells (Novagen), using pET expression vectors (Novagen). Cultures were grown at 37°C to an OD_{600} of 0.8. Expression was induced by addition of 0.5 mM IPTG, and cells were subsequently incubated at 18°C overnight, with shaking. After harvesting, resuspended cells were disrupted by sonication. All recombinant proteins were purified to homogeneity using metal affinity (QIAGEN) or Strep-Tactin fast flow (IBA), ion exchange, and gel filtration chromatography with standard protocols (GE Healthcare).

ATPase Assays

ATPase assay reaction mixtures (50 μl) contained 20 mM Tris-HCl (pH 7.5), 8 mM DTT, 5 mM $MgCl_2$, 10 mM KCl, 4% (w/v) glycerol, 80 μg/ml BSA, and the specified RNA (10 ng/μl) plus a trace amount of [γ-^{32}P]ATP (2 nM) mixed with different amounts of nonradioactive ATP and 20 nM enzyme. The

luciferase assay after 18 hr (fold induction compared to mock-treated empty vector control). Mean values and standard deviations (error bars) of three independent experiments are shown.

(F) Proposed model for RNA 5′-triphosphate (gray with red phosphates) activation of RIG-I by ligand-induced dimer formation of RD (yellow with magenta zinc ion). RNA stoichiometry and domain-domain interactions are tentative.

reactions were initiated by the addition of enzyme and incubated at 37°C. Samples (1 μl) were removed at 3 min intervals and evaluated by thin-layer chromatography. k_{cat} and V_{max} values were calculated by nonlinear curve fitting of multiple (two to five) independent determinations (see Table S2).

Molecular Weight Determination by Size-Exclusion Chromatography and Light Scattering

Assays were done on a GE Äcta system equipped with a Superose 6 10/300 (GE Healthcare) gel filtration column and connected to a Viscotek VE 3580 RI detector and Viscotek 270 DUAL detector. The gel filtration buffer was 30 mM Tris-HCl (pH 7.5), 150 mM NaCl, 2 mM DTT, and 10 μM $ZnCl_2$. UV absorption, refractive index, and low angle light scattering signals were collected. The system was calibrated with BSA (MW 67,000 Da) standard solution with a concentration of 2 mg/ml.

Fluorescence and Anisotropy Measurement

Fluorescence anisotropy experiments were performed with a FluoroMax-P fluorimeter (HORIBA Jobin Yvon), equipped with a Glan-Thompson prism polarizer. Typically, 1.2 ml of buffer (30 mM Tris-HCl [pH 7.5], 150 mM NaCl, 2 mM DTT, and 10 μM $ZnCl_2$) and 50 nM RNA (in vitro-transcribed pppRVL with incorporated Alexa Fluor 488-5-UTP) were pre-equilibrated in a quartz cuvette at 12°C. Protein samples were added in a stepwise manner and briefly mixed by magnetic stirring. After 3 min re-equilibration, the anisotropy data were collected using an excitation wavelength of 492 nm and monitoring the emission 516 nm. The band pass was 5 nm for excitation and 5 nm for emission. A maximum number of ten trials were performed until less than 2% deviation of the signal was reached.

In Vivo RD Titration Experiments

Reporter gene assays for activation of IFN-β promoter were performed in HEK293T cells seeded in 24-well plates. At a confluence of 75%, cells were transfected with 100 ng IFN-β firefly reporter plasmid (p125luc) and 1 ng of a plasmid encoding CMV-controlled renilla luciferase (pRL-CMV, Promega) as a control, using Lipofectamine 2000 (Invitrogen). In addition, cells were transfected with 100 ng of pEF-BOS-RIG-I full-length plasmid and the indicated increasing amounts of pCAGGS-RIG-I RD expression construct. Twenty-four hours after DNA transfection, cells were transfected with 200 ng in vitro-transcribed pppRVL to stimulate IFN production. Cells were lysed after 24 hr incubation and analyzed for dual reporter gene activity according to the supplier's instructions (Promega) in a Luminometer (Berthold).

In Vivo Analysis of RIG-I Mutants

HEK293 cells (DSMZ, Braunschweig, Germany) were maintained in DMEM with supplements (0.6 g/l L-Glu, 10% FBS, and 1% Pen/Strep from GIBCO-Invitrogen, Karlsruhe, Germany). BHK21 cells (ATCC) were grown in Glasgow medium supplemented with 0.6 g/l L-Glu, 10% FBS, 1% Pen/Strep, and 1% tryptose broth (GIBCO-Invitrogen). Cell cultures were incubated at 37°C with 5% CO_2. VSV-M51R mutant was kindly provided by O. Ebert (TU Munich). Virus stock and plaque assay on BHK21 cells have been described. Mutants of Flag-RIG-I (kindly provided by T. Fujita) were generated using the QuikChange Site-Directed Mutagenesis Kit (Stratagene, Amsterdam, Netherlands) and sequenced. HEK293 cells (2×10^5 cells/24-well) were transiently transfected with 10 ng of pRL-TK reporter (renilla luciferase under control of TK promoter, Promega, Mannheim, Germany), 100 ng of pIFN-β-Luc (firefly luciferase under control of mIFN-β promoter, kindly provided by T. Taniguchi), and 10, 100, or 400 ng of RIG-I constructs or empty control vector using Lipofectamine 2000 (Invitrogen, Karlsruhe, Germany). Eighteen hours after transfection, cells were either infected with 10 moi VSV-M51R or transfected with 1 μg/ml in vitro-transcribed pppVSVL or RNA isolated from mock-infected and VSV-infected cells using Lipofectamine 2000. Cell extracts were prepared and assayed in the Dual Luciferase Reporter System (Promega) after 18 hr.

RNA Pull-Down Experiments

5′-triphosphate RNA encompassing the VSV leader RNA sequence (pppVSVL) was generated by in vitro transcription from a template DNA generated by PCR using plasmid rVSV-EGFP (kindly provided by O. Ebert) as template and 5′ T7 primer (MAXIscript T7 Kit, Ambion, Huntingdon, UK). The DNA template was removed by DNase I treatment, and RNA was purified using Nuc Away Columns (Ambion). For removal of 5′-triphosphates, 20 μg of RNA was treated with 30 U CIAP (NEB, Frankfurt/Main, Germany) for 2 hr at 37°C in the presence of RNase inhibitor (Fermentas, St. Leon, Germany) and extracted with phenol-chloroform. Biotinylated pppVSVL was transcribed from the template DNA described above by using the AmpliScribe Flash T7 Kit (Epicenter, Madison, USA) and biotin-16-uridine-5′-triphosphate (Roche, Mannheim, Germany). RNA binding assays were performed as described (Saito et al., 2007): cytoplasmic extracts were prepared from 3×10^8 HEK293 cells transfected with Flag-RIG-I plasmids. The extracts were incubated with biotinylated pppVSVL and subjected to pull-down with streptavidin agarose beads (Sigma-Aldrich, Munich, Germany), followed by SDS-PAGE analysis and immunoblotting with anti-Flag M2 antibody (Sigma-Aldrich, Munich, Germany).

Crystallization and Structure Determination

RD was crystallized by mixing 2 μl protein (20 mg ml^{-1} in 30 mM Tris-HCl [pH 7.5], 150 mM NaCl, 2 mM DTT, and 10 μM $ZnCl_2$) with 2 μl buffer containing 0.1 M CHES (pH 10.0) and 18% w/v PEG 8000 in a sitting drop vapor diffusion system at 20°C. The derivative used for phase determination was prepared by soaking the crystals for 10 min in 2 mM mercury acetate, 0.1 M CHES (pH 10.0), and 18% w/v PEG 8000. Cryocooling was achieved by soaking the crystals for 5–10 s in reservoir solution containing 15% D(-)-2,3-butanediol and flash-freezing in liquid nitrogen. Highly redundant multiwavelength anomalous dispersion (MAD) data to 2.7 Å on mercury-containing and to 3 Å on native crystals were collected at beamlines PX SLS (Villigen, Switzerland) and ID23-2, ESRF (Grenoble, France). The data sets were processed with XDS (Kabsch, 1993). The space group was identified as P21, and 10 molecules were found per asymmetric unit. One mercury atom was located per molecule and initial phases were calculated and refined with the program AUTOSHARP (Global Phasing, Cambridge), leading to an interpretable electron density map. The manual model building was carried out by using the program Coot (Emsley and Cowtan, 2004). Prior to model building and refinement, we randomly omitted 10% of the reflections for monitoring the free R value. Refinement was performed with CNS V.1.1 (Brunger et al., 1998) and included overall anisotropic B factor and bulk solvent corrections, individual B factor refinement, simulated annealing, and positional refinement. Initial NCS restraints were gradually removed in the final cycles of the refinement, to allow some structural variations. Data collection and model statistics are summarized in Table 1. Figures were prepared with PyMOL (DeLano Scientific).

Supplemental Data

Supplemental Data include eight figures and three tables and can be found with this article online at http://www.molecule.org/cgi/content/full/29/2/169/DC1/.

ACKNOWLEDGMENTS

We thank Wolfgang Reindl for experimental help and Imre Berger for help with the MultiBac expression system. We thank the staffs of PXI (Swiss Light Source, Villingen) and ID14 (European Synchrotron Radiation Facility, Grenoble) for beam time allowance and help with data collection. This work was supported by the German Research Council DFG Sonderforschungsbereich 455 to K.-P.H., A. Krug, and K.-K.C. and by the Center for Integrated Protein Science and Munich Center for Advanced Photonics to K.-P.H. A. Kirchhofer acknowledges support by the DFG Graduate School 1202. This work is part of the theses of K.E. and A. Kirchhofer.

Received: April 6, 2007
Revised: July 12, 2007
Accepted: October 24, 2007
Published: January 31, 2008

REFERENCES

Akira, S., Uematsu, S., and Takeuchi, O. (2006). Pathogen recognition and innate immunity. Cell *124*, 783–801.

Berger, I., Fitzgerald, D.J., and Richmond, T.J. (2004). Baculovirus expression system for heterologous multiprotein complexes. Nat. Biotechnol. *22*, 1583–1587.

Brunger, A.T., Adams, P.D., Clore, G.M., DeLano, W.L., Gros, P., Grosse-Kunstleve, R.W., Jiang, J.S., Kuszewski, J., Nilges, M., Pannu, N.S., et al. (1998). Crystallography & NMR system: a new software suite for macromolecular structure determination. Acta Crystallogr. D Biol. Crystallogr. *54*, 905–921.

Emsley, P., and Cowtan, K. (2004). Coot: model-building tools for molecular graphics. Acta Crystallogr. D Biol. Crystallogr. *60*, 2126–2132.

Gitlin, L., Barchet, W., Gilfillan, S., Cella, M., Beutler, B., Flavell, R.A., Diamond, M.S., and Colonna, M. (2006). Essential role of mda-5 in type I IFN responses to polyriboinosinic:polyribocytidylic acid and encephalomyocarditis picornavirus. Proc. Natl. Acad. Sci. USA *103*, 8459–8464.

Gorbalenya, A.E., Koonin, E.V., Donchenko, A.P., and Blinov, V.M. (1988). A novel superfamily of nucleoside triphosphate-binding motif containing proteins which are probably involved in duplex unwinding in DNA and RNA replication and recombination. FEBS Lett. *235*, 16–24.

Hiscott, J., Lin, R., Nakhaei, P., and Paz, S. (2006). MasterCARD: a priceless link to innate immunity. Trends Mol. Med. *12*, 53–56.

Holm, L., and Sander, C. (1993). Protein structure comparison by alignment of distance matrices. J. Mol. Biol. *233*, 123–138.

Hopfner, K.P., and Tainer, J.A. (2003). Rad50/SMC proteins and ABC transporters: unifying concepts from high-resolution structures. Curr. Opin. Struct. Biol. *13*, 249–255.

Hopfner, K.P., and Michaelis, J. (2007). Mechanisms of nucleic acid translocases: lessons from structural biology and single-molecule biophysics. Curr. Opin. Struct. Biol. *17*, 87–95.

Hornung, V., Ellegast, J., Kim, S., Brzozka, K., Jung, A., Kato, H., Poeck, H., Akira, S., Conzelmann, K.K., Schlee, M., et al. (2006). 5′-triphosphate RNA is the ligand for RIG-I. Science *314*, 994–997.

Itzen, A., Pylypenko, O., Goody, R.S., Alexandrov, K., and Rak, A. (2006). Nucleotide exchange via local protein unfolding—structure of Rab8 in complex with MSS4. EMBO J. *25*, 1445–1455.

Johnson, C.L., and Gale, M., Jr. (2006). CARD games between virus and host get a new player. Trends Immunol. *27*, 1–4.

Kabsch, W. (1993). Automatic processing of rotation diffraction data from crystals of initially unknown symmetry and cell constants. J. Appl. Crystallogr. *21*, 916–924.

Kato, H., Takeuchi, O., Sato, S., Yoneyama, M., Yamamoto, M., Matsui, K., Uematsu, S., Jung, A., Kawai, T., Ishii, K.J., et al. (2006). Differential roles of MDA5 and RIG-I helicases in the recognition of RNA viruses. Nature *441*, 101–105.

Kawai, T., and Akira, S. (2006). Innate immune recognition of viral infection. Nat. Immunol. *7*, 131–137.

Kawai, T., Takahashi, K., Sato, S., Coban, C., Kumar, H., Kato, H., Ishii, K.J., Takeuchi, O., and Akira, S. (2005). IPS-1, an adaptor triggering RIG-I- and Mda5-mediated type I interferon induction. Nat. Immunol. *6*, 981–988.

Komuro, A., and Horvath, C.M. (2006). RNA- and virus-independent inhibition of antiviral signaling by RNA helicase LGP2. J. Virol. *80*, 12332–12342.

Meylan, E., Curran, J., Hofmann, K., Moradpour, D., Binder, M., Bartenschlager, R., and Tschopp, J. (2005). Cardif is an adaptor protein in the RIG-I antiviral pathway and is targeted by hepatitis C virus. Nature *437*, 1167–1172.

Meylan, E., Tschopp, J., and Karin, M. (2006). Intracellular pattern recognition receptors in the host response. Nature *442*, 39–44.

Pichlmair, A., Schulz, O., Tan, C.P., Naslund, T.I., Liljestrom, P., Weber, F., and Reis e Sousa, C. (2006). RIG-I-mediated antiviral responses to single-stranded RNA bearing 5′-phosphates. Science *314*, 997–1001.

Plumet, S., Herschke, F., Bourhis, J.M., Valentin, H., Longhi, S., and Gerlier, D. (2007). Cytosolic 5′-triphosphate ended viral leader transcript of measles virus as activator of the RIG I-mediated interferon response. PLoS ONE *2*, e279. 10.1371/journal.pone.0000279.

Rothenfusser, S., Goutagny, N., DiPerna, G., Gong, M., Monks, B.G., Schoenemeyer, A., Yamamoto, M., Akira, S., and Fitzgerald, K.A. (2005). The RNA helicase Lgp2 inhibits TLR-independent sensing of viral replication by retinoic acid-inducible gene-I. J. Immunol. *175*, 5260–5268.

Saito, T., Hirai, R., Loo, Y.M., Owen, D., Johnson, C.L., Sinha, S.C., Akira, S., Fujita, T., and Gale, M., Jr. (2007). Regulation of innate antiviral defenses through a shared repressor domain in RIG-I and LGP2. Proc. Natl. Acad. Sci. USA *104*, 582–587.

Seth, R.B., Sun, L., Ea, C.K., and Chen, Z.J. (2005). Identification and characterization of MAVS, a mitochondrial antiviral signaling protein that activates NF-kappaB and IRF 3. Cell *122*, 669–682.

Seth, R.B., Sun, L., and Chen, Z.J. (2006). Antiviral innate immunity pathways. Cell Res. *16*, 141–147.

Sumpter, R., Jr., Loo, Y.M., Foy, E., Li, K., Yoneyama, M., Fujita, T., Lemon, S.M., and Gale, M., Jr. (2005). Regulating intracellular antiviral defense and permissiveness to hepatitis C virus RNA replication through a cellular RNA helicase, RIG-I. J. Virol. *79*, 2689–2699.

Xu, L.G., Wang, Y.Y., Han, K.J., Li, L.Y., Zhai, Z., and Shu, H.B. (2005). VISA is an adapter protein required for virus-triggered IFN-beta signaling. Mol. Cell *19*, 727–740.

Yoneyama, M., Kikuchi, M., Natsukawa, T., Shinobu, N., Imaizumi, T., Miyagishi, M., Taira, K., Akira, S., and Fujita, T. (2004). The RNA helicase RIG-I has an essential function in double-stranded RNA-induced innate antiviral responses. Nat. Immunol. *5*, 730–737.

Yoneyama, M., Kikuchi, M., Matsumoto, K., Imaizumi, T., Miyagishi, M., Taira, K., Foy, E., Loo, Y.M., Gale, M., Jr., Akira, S., et al. (2005). Shared and unique functions of the DExD/H-box helicases RIG-I, MDA5, and LGP2 in antiviral innate immunity. J. Immunol. *175*, 2851–2858.

Yu, H., and Schreiber, S.L. (1995). Structure of guanine-nucleotide-exchange factor human Mss4 and identification of its Rab-interacting surface. Nature *376*, 788–791.

Accession Numbers

The Protein Data Bank (PDB) accession number for coordinates and structure factors of zinc-bound RD is 2QFB. The PDB accession number for coordinates and structure factors of mercury-bound RD is 2QFD.

JOURNAL OF VIROLOGY, Oct. 2008, p. 9639–9646 Vol. 82, No. 19
0022-538X/08/$08.00+0 doi:10.1128/JVI.00351-08

The DNA Damage Sensors Ataxia-Telangiectasia Mutated Kinase and Checkpoint Kinase 2 Are Required for Hepatitis C Virus RNA Replication[▽]

Yasuo Ariumi,[1] Misao Kuroki,[1] Hiromichi Dansako,[1] Ken-Ichi Abe,[1] Masanori Ikeda,[1] Takaji Wakita,[2] and Nobuyuki Kato[1]*

Department of Molecular Biology, Okayama University Graduate School of Medicine, Dentistry, and Pharmaceutical Sciences, 2-5-1, Shikata-cho, Okayama 700-8558, Japan,[1] and Department of Virology II, National Institute of Infectious Diseases, 1-23-1 Toyama, Shinjuku-ku, Tokyo 162-8640, Japan[2]

Received 18 February 2008/Accepted 18 July 2008

Cellular responses to DNA damage are crucial for maintaining genome integrity, virus infection, and preventing the development of cancer. Hepatitis C virus (HCV) infection and the expression of the HCV nonstructural protein NS3 and core protein have been proposed as factors involved in the induction of double-stranded DNA breaks and enhancement of the mutation frequency of cellular genes. Since DNA damage sensors, such as the ataxia-telangiectasia mutated kinase (ATM), ATM- and Rad3-related kinase (ATR), poly(ADP-ribose) polymerase 1 (PARP-1), and checkpoint kinase 2 (Chk2), play central roles in the response to genotoxic stress, we hypothesized that these sensors might affect HCV replication. To test this hypothesis, we examined the level of HCV RNA in HuH-7-derived cells stably expressing short hairpin RNA targeted to ATM, ATR, PARP-1, or Chk2. Consequently, we found that replication of both genome-length HCV RNA (HCV-O, genotype 1b) and the subgenomic replicon RNA were notably suppressed in ATM- or Chk2-knockdown cells. In addition, the RNA replication of HCV-JFH1 (genotype 2a) and the release of core protein into the culture supernatants were suppressed in these knockdown cells after inoculation of the cell culture-generated HCV. Consistent with these observations, ATM kinase inhibitor could suppress the HCV RNA replication. Furthermore, we observed that HCV NS3-NS4A interacted with ATM and that HCV NS5B interacted with both ATM and Chk2. Taken together, these results suggest that the ATM signaling pathway is critical for HCV RNA replication and may represent a novel target for the clinical treatment of patients with chronic hepatitis C.

Hepatitis C virus (HCV) infection frequently causes chronic hepatitis, which progresses to liver cirrhosis and hepatocellular carcinoma. HCV infection has now become a serious health problem, with at least 170 million people currently infected worldwide (28). HCV is an enveloped virus with a positive single-stranded 9.6-kb RNA genome, which encodes a large polyprotein precursor of approximately 3,000 amino acid residues. This polyprotein is cleaved by a combination of the host and viral proteases into at least 10 proteins in the following order: core, envelope 1 (E1), E2, p7, nonstructural 2 (NS2), NS3, NS4A, NS4B, NS5A, and NS5B (12, 13, 27).

Studies have shown that various viruses with distinct replication strategies—including the DNA viruses Epstein-Barr virus, herpes simplex virus 1, adenovirus, and simian virus 40 and the retrovirus human immunodeficiency virus type 1 (HIV-1)—can activate DNA damage response pathways and utilize these damage responses to facilitate their own viral reproduction and promote the survival of infected cells (2, 16, 17). In the case of HCV, it has been proposed that HCV infection causes double-stranded DNA (dsDNA) breaks and enhances the mutation frequency of cellular genes and that these effects are mediated by nitric oxide (18, 19). In addition, the HCV core, E1, and NS3 proteins have been suggested to be potent reactive oxygen species inducers, leading to DNA damage (19). Furthermore, we previously demonstrated that HCV NS5B-expressing PH5CH8 immortalized human hepatocyte cells were susceptible to DNA damage in the form of dsDNA breaks (23). Thus, HCV seems to be associated with the dsDNA damage response pathways.

Since the DNA damage sensors, such as ataxia-telangiectasia mutated kinase (ATM), ATM- and Rad3-related kinase (ATR), poly(ADP-ribose) polymerase 1 (PARP-1), and checkpoint kinase 2 (Chk2; a direct downstream target of ATM), play central roles in response to genotoxic stress (10), we hypothesized that these sensors might affect HCV replication.

To investigate the possible involvement of these cellular factors in HCV replication, we examined the level of HCV RNA in cells rendered defective for DNA damage sensors by RNA interference or by pharmacological inhibition.

MATERIALS AND METHODS

Cell culture. 293FT cells were cultured in Dulbecco's modified Eagle's medium (DMEM; Invitrogen, Carlsbad, CA) supplemented with 10% fetal bovine serum (FBS). The HuH-7-derived O cells harboring a replicative genome-length HCV RNA and the HuH-7-derived sO cells harboring the subgenomic replicon RNA of HCV-O were cultured in DMEM with 10% FBS and G418 (300 μg/ml geneticin; Invitrogen) as described previously (11, 14). Oc and sOc cells, which were created by eliminating HCV RNA from O cells and sO cells by interferon (IFN) treatment (11, 14), respectively, were also cultured in DMEM with 10% FBS.

RNA interference. Oligonucleotides with the following sense and antisense sequences were used for the cloning of short hairpin RNA (shRNA)-encoding se-

* Corresponding author. Mailing address: Department of Molecular Biology, Okayama University Graduate School of Medicine, Dentistry, and Pharmaceutical Sciences, 2-5-1, Shikata-cho, Okayama 700-8558, Japan. Phone: 81 86 235 7385. Fax: 81 86 235 7392. E-mail: nkato@md.okayama-u.ac.jp.

▽ Published ahead of print on 30 July 2008.

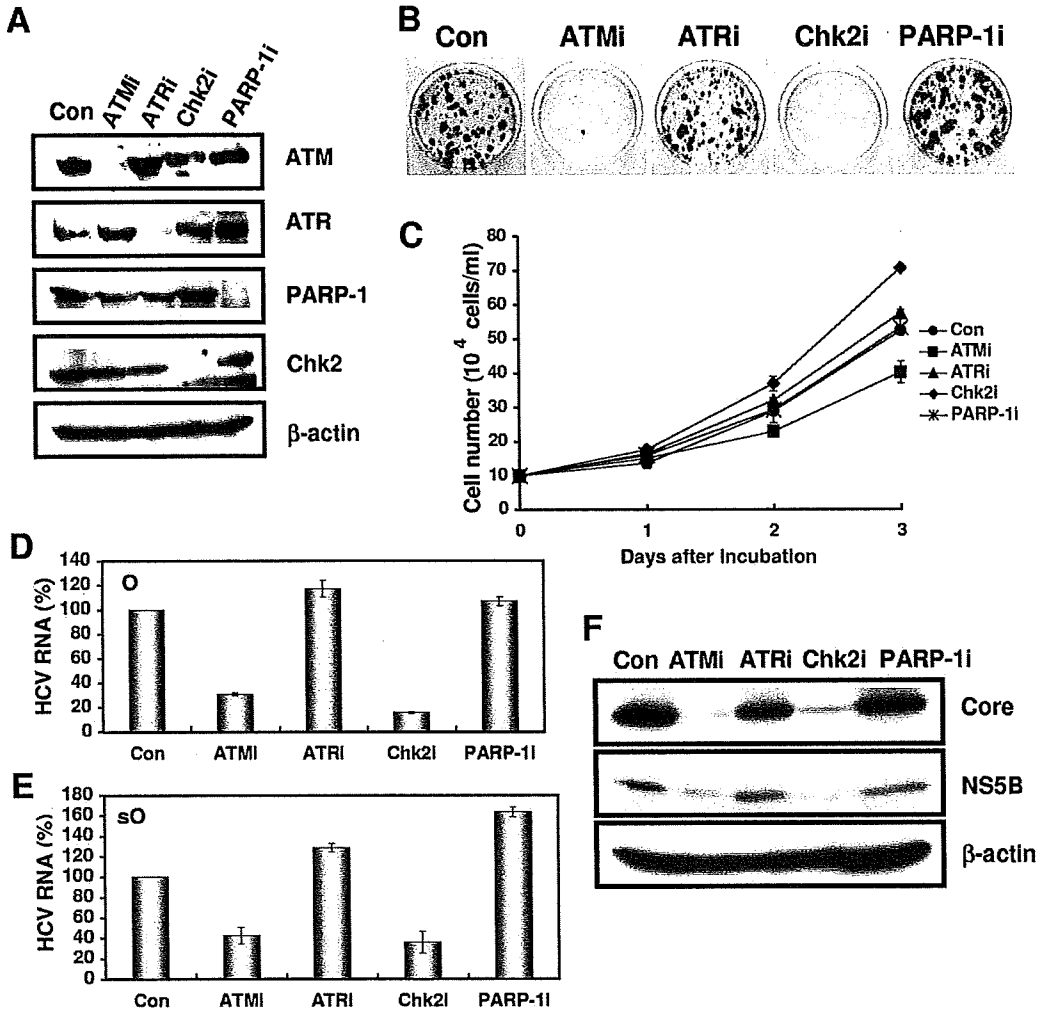

FIG. 1. The ATM signaling pathway is required for HCV RNA replication. (A) Inhibition of ATM, ATR, Chk2, or PARP-1 expression by shRNA-producing lentiviral vectors. The results of the Western blot analysis of cellular lysates with anti-ATM, anti-ATR, anti-Chk2, anti-PARP-1, or anti-β-actin antibody in Oc cells expressing shRNA targeted to ATM (ATMi), ATR (ATRi), Chk2 (Chk2i), or PARP-1 (PARP-1i) as well as in Oc cells transduced with a control lentiviral vector (Con) are shown. (B) ECF in ATM-, ATR-, Chk2-, or PARP-1-knockdown cells. In vitro transcribed ON/C-5B K1609E RNA (2 μg) was transfected into the ATM-, ATR-, Chk2, or PARP-1-knockdown Oc cells or the Oc cells transduced with a control lentiviral vector (Con). G418-resistant colonies were stained with Coomassie brilliant blue at 3 weeks after electroporation of RNA. Experiments were done in duplicate, and a representative result is shown. (C) The cell growth curve of ATM (ATMi), ATR (ATRi), Chk2 (Chk2i), or PARP-1 (PARP-1i)-knockdown Oc cells or the Oc cells transduced with a control lentiviral vector (Con). Results from three independent experiments are shown. (D) The level of genome-length HCV-O RNA was monitored by real-time LightCycler PCR (Roche). Experiments were done in triplicate, and columns represent the mean percentage of HCV RNA. (E) The level of subgenomic replicon (sO cells) RNA was monitored by real-time LightCycler PCR. Results from three independent experiments are shown as described in panel D. (F) The HCV core or NS5B protein expression level in ATM-, ATR-, Chk2-, or PARP-1-knockdown cells. The results of Western blot analysis of cellular lysates with anti-HCV core protein, anti-HCV NS5B, or anti-β-actin antibody in O cells expressing shRNA targeted to ATM (ATMi), ATR (ATRi), Chk2 (Chk2i), or PARP-1 (PARP-1i) as well as in O cells transduced with a control lentiviral vector (Con) are shown.

quences targeted to Chk2 in lentiviral vector: 5′-GATCCCCGGGGGAGAGCTGTT TGACATTCAAGAGATGTCAAACAGCTCTCCCCCTTTTTGGAAA-3′ (sense) and 5′-AGCTTTTCCAAAAAGGGGGAGAGCTGTTTGACATCTCTTGAATGT CAAACAGCTCTCCCCCGGG-3′ (antisense). The oligonucleotides above were annealed and subcloned into the BglII-HindIII site, downstream from an RNA polymerase III promoter of pSUPER (5), generating pSUPER-Chk2i. To construct pLV-Chk2i, the BamHI-SalI fragments of the pSUPER-Chk2i were subcloned into the BamHI-SalI site of pRDI292, an HIV-1-derived self-inactivating lentiviral vector containing a puromycin resistance marker allowing for the selection of transduced cells (4). pLV-ATMi, pLV-ATRi, and pLV-PARP-1i were constructed as described previously (1).

Lentiviral vector production. The vesicular stomatitis virus G protein (VSV-G)-pseudotyped HIV-1-based vector system has been described previously (24). The lentiviral vector particles were produced by transient transfection of the second-generation packaging construct pCMV-ΔR8.91 (30) and the VSV-G envelope plasmid pMDG2 as well as the lentiviral vector into 293FT cells with FuGene6 (Roche Diagnostics, Mannheim, Germany).

Quantitative reverse transcription-PCR analysis. Quantitative reverse transcription-PCR analysis for HCV RNA was performed by real-time LightCycler PCR as described previously (11).

Western blot analysis. Cells were lysed in buffer containing 50 mM Tris-HCl (pH 8.0), 150 mM NaCl, 4 mM EDTA, 1% Nonidet P-40, 0.1% sodium dodecyl sulfate (SDS), 1 mM dithiothreitol, and 1 mM phenylmethylsulfonyl fluoride. Supernatants from these lysates were subjected to SDS-polyacrylamide gel electrophoresis, followed by immunoblotting analysis using anti-ATM (2C1; GTX70103 [GeneTex, San Antonio, TX]), anti-ATR (GTX70133; GeneTex), anti-Chk2 (NT; ProSci, Poway, CA), anti-Chk2 (DCS-273; Medical and Biological Laboratories, Nagoya, Japan), anti-phospho-Chk2 (Thr68) (Cell Signaling,

Danvers, MA), anti-PARP-1 (C-2-10; Calbiochem, Merck Biosciences, Darmstadt, Germany), anti-hemagglutinin (HA) (HA-7; Sigma, St. Louis, MO), anti-core protein (CP-9 and CP-11; Institute of Immunology, Tokyo, Japan), anti-NS3 and anti-NS5B (no. 14; a generous gift from M. Kohara, the Tokyo Metropolitan Institute of Medical Science, Japan), anti-NS5A (no. 8926; a generous gift from A. Takamizawa, The Research Foundation for Microbial Diseases of Osaka University, Japan), and anti-β-actin (Sigma) Antibodies.

Immunofluorescence and confocal microscopic analysis. Cells were fixed in 3.5% formaldehyde in phosphate-buffered saline (PBS) and permeabilized in 0.1% NP-40 in PBS at room temperature. Cells were incubated with anti-ATM antibody (5C2; GTX70107 [GeneTex] or PM026 [MBL]), anti-HA antibody (3F10), anti-NS5B antibody and/or anti-NS3 antibody at a 1:300 dilution in PBS containing 3% bovine serum albumin at 37°C for 30 min. Cells were then stained with fluorescein isothiocyanate (FITC)-conjugated anti-rabbit antibody (Jackson ImmunoResearch, West Grove, PA) or anti-Cy3-conjugated anti-mouse antibody (Jackson ImmunoResearch) at a 1:300 dilution in PBS containing bovine serum albumin at 37°C for 30 min. Following extensive washing in PBS, cells were mounted on slides using a mounting medium of 90% glycerin–10% PBS with 0.01% *p*-phenylenediamine added to reduce fading. Samples were viewed under a confocal laser-scanning microscope (LSM510; Zeiss, Jena, Germany).

Immunoprecipitation. Cells were lysed in buffer containing 10 mM Tris-HCl (pH 8.0), 150 mM NaCl, 4 mM EDTA, 0.5% NP-40, 10 mM NaF, 1 mM dithiothreitol, and 1 mM phenylmethylsulfonyl fluoride. Lysates were precleared with 30 μl of protein G-Sepharose (GE Healthcare Biosciences, Uppsala, Sweden). Precleared supernatants were incubated with 5 μg of anti-HA antibody (3F10; Roche), 10 μl of anti-NS5B antibody, 5 μg of anti-Chk2 antibody (DCS-273; MBL), 5 μg of anti-FLAG antibody (M2; Sigma), or 5 μg of anti-ATM antibody (2C1) (GTX70103; GeneTex) at 4°C for 1 h. Following absorption of the precipitates on 30 μl of protein G-Sepharose resin for 1 h, the resin was washed four times with 700 μl of lysis buffer. Proteins were eluted by boiling the resin for 5 min in 2× Laemmli sample buffer. The proteins were then subjected to SDS-polyacrylamide gel electrophoresis, followed by immunoblotting analysis using anti-ATM, anti-Chk2, anti-HCV core protein (CP-9 and CP-11 mixture), anti-NS5A, anti-NS5B, anti-HA (HA-7; Sigma), or anti-NS3 antibody.

RESULTS

ATM and Chk2 are required for HCV RNA replication. To determine the potential role of DNA damage sensors in HCV replication, we first used lentiviral vector-mediated RNA interference to stably knockdown ATM, ATR, PARP-1 (1), or Chk2 in the following human hepatoma HuH-7-derived cell lines: O cells harboring a replicative genome-length HCV RNA (HCV-O, genotype 1b) (11), Oc cells derived from O cells (created by eliminating genome-length HCV RNA from O cells by IFN treatment) (11), sO cells harboring the subgenomic replicon of HCV-O (14), or RSc cells that cell culture-generated HCV (HCVcc) (JFH1, genotype 2a) (29) could infect and effectively replicate (3). To express shRNAs targeted to ATM, ATR, PARP-1 (1), or Chk2, we used a VSV-G-pseudotyped HIV-1-based vector system (24). We used puromycin-resistant pooled cells 10 days after the lentiviral transduction in all experiments. Western blot analysis of the lysates demonstrated very effective knockdown of ATM, ATR, Chk2, and PARP-1 in Oc cells (Fig. 1A). The effective knockdown of ATM, ATR, Chk2, or PARP-1 in O cells or sO cells was also confirmed by Western blot analysis (data not shown). In this context, the efficiency of colony formation (ECF) in ATM- or Chk2-, but not ATR- or PARP-1-, knockdown Oc cells transfected with the genome-length HCV-O RNA with an adapted mutation at amino acid position 1609 in the NS3 helicase region (ON/C-5B K1609E RNA) (11) was notably reduced compared with the control cells (Fig. 1B) even though Chk2-knockdown cells had a slightly faster growth rate than the control cells (Fig. 1C), suggesting that both ATM and Chk2 are crucial for HCV RNA replication. To further confirm this

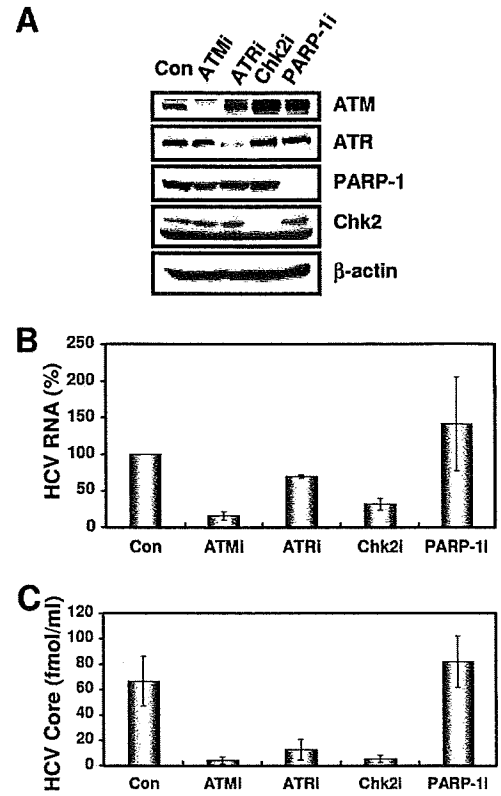

FIG. 2. ATM affects HCV infection. (A) Inhibition of ATM, ATR, Chk2, or PARP-1 expression by shRNA-producing lentiviral vectors. The results of Western blot analysis of cellular lysates with anti-ATM, anti-ATR, anti-PARP-1, anti-Chk2, or anti-β-actin antibody in RSc cured cells expressing shRNA targeted to ATM (ATMi), ATR (ATRi), Chk2 (Chk2i), or PARP-1 (PARP-1i) as well as in RSc cells transduced with a control lentiviral vector (Con) are shown. (B) The level of genome-length HCV (JFH1) RNA was monitored by real-time LightCycler PCR after inoculation of the HCVcc. Results from three independent experiments are shown as described in the legend of Fig. 1D. (C) The levels of the core protein in the culture supernatants were determined by enzyme-linked immunosorbent assay (Mitsubishi Kagaku Bio-Clinical Laboratories). Experiments were done in triplicate, and columns represent the mean core protein levels.

observation, we quantitatively examined the level of HCV RNA in the O cell- or sO cell-derived knockdown cells. Consequently, we found that replication of both genome-length HCV RNA (HCV-O) and its subgenomic replicon RNA (sO) were notably suppressed in ATM- or Chk2-knockdown cells but not in ATR- or PARP-1-knockdown cells (Fig. 1D and E). Consistent with this finding, the expression levels of core and NS5B proteins were also significantly decreased in the cell lysates of ATM- or Chk2-knockdown O cells (Fig. 1F). We next examined the replication level of HCV-JFH1 in ATM-, ATR-, Chk2-, or PARP-1-knockdown RSc cells (Fig. 2A). The results revealed that RNA replication of HCV-JFH1 and release of core protein into the culture supernatants were suppressed in only ATM- or Chk2-knockdown RSc cells after inoculation with HCVcc (Fig. 2B and C). Interestingly, the release of core protein into the culture supernatant was also significantly suppressed in ATR-knockdown RSc cells, while HCV RNA replication was slightly suppressed in these cells

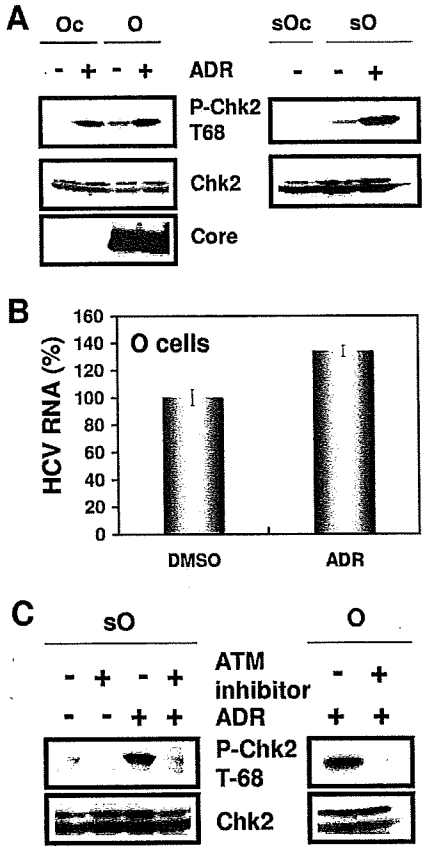

FIG. 3. ATM-dependent DNA damage response in HCV RNA-replicating cells. (A) Stimulation of Chk2 phosphorylation in the HCV RNA-replicating cells. The Oc, O, or sO cells were treated with 100 nM adriamycin (Sigma) for 2 h. The results of Western blot analysis of cellular lysates with anti-phospho-Chk2 (Thr68) (P-Chk2 T68), anti-Chk2, or anti-core protein antibody are shown. (B) Effect of adriamycin on HCV RNA replication. The O cells were treated with 100 nM adriamycin for 24 h. The level of genome-length HCV-O RNA was monitored by real-time LightCycler PCR. Results from three independent experiments are shown as described in the legend of Fig. 1D. DMSO, dimethyl sulfoxide. (C) Effect of ATM kinase inhibitor on Chk2 phosphorylation. The sO or O cells were pretreated with 10 μM ATM kinase inhibitor (KU-55933) (Calbiochem) for 2 h, followed by treatment with 100 nM adriamycin for 2 h. The results of Western blot analysis of cellular lysates with anti-phospho-Chk2 (Thr68) or anti-Chk2 antibody are shown.

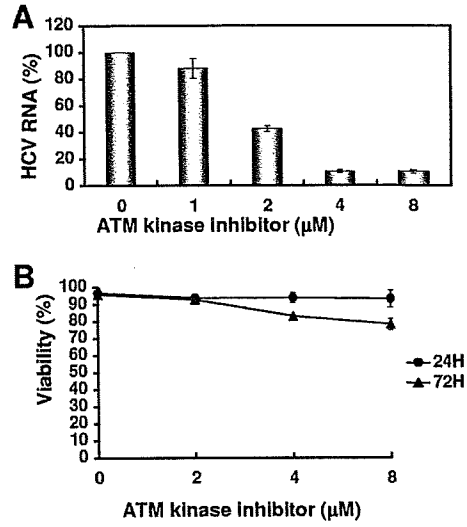

FIG. 4. Suppression of HCV RNA replication by ATM kinase inhibitor. (A) The level of genome-length HCV-O RNA was monitored by real-time LightCycler PCR after treatment with the indicated concentration of ATM kinase inhibitor for 72 h. Results from three independent experiments are shown as described in the legend of Fig. 1D. (B) Cell viabilities after treatment with the indicated concentration of ATM kinase inhibitor for 24 h or 72 h are shown.

(Fig. 2B and C), suggesting that ATR participates in the production of HCV virion.

In contrast, highly efficient knockdown of PARP-1 had no observable effects on the ECF (Fig. 1B), HCV RNA replication (Fig. 1D and E and 2B), or core protein expression in the cell lysate or in the supernatant (Fig. 1F and 2C), suggesting that our finding was not due to a nonspecific event. Thus, we have demonstrated for the first time that DNA damage sensors, ATM and Chk2, are required for HCV RNA replication.

ATM kinase activity in HCV RNA-replicating cells. Although it has been proposed that HCV causes dsDNA breaks (18, 19), little is known about whether HCV activates or inhibits the ATM-dependent damage response pathway. In this regard, it is worth noting that we observed weak but significant Chk2 phosphorylation at threonine 68, the specific marker for ATM activation (20, 21), in the HCV RNA-replicating cells (O and sO cells) but not in the HCV-negative Oc and sOc cells (created by eliminating replicon RNA from sO cells by IFN treatment) (Fig. 3A), suggesting that the persistent HCV RNA replication stimulated the ATM-dependent DNA damage response. Furthermore, a 2-h treatment with 100 nM adriamycin, a dsDNA break inducer, markedly induced Chk2 phosphorylation in Oc, O, and sO cells (Fig. 3A). Importantly, Chk2 phosphorylation was not inhibited even in the HCV RNA-replicating cells (O and sO cells) (Fig. 3A), suggesting that the persistent HCV RNA replication and the HCV proteins are not able to suppress the ATM-dependent DNA damage response. To examine whether such a DNA damage response activates HCV RNA replication, we quantified the level of HCV RNA in the O cells treated with 100 nM adriamycin for 24 h. The results show that HCV RNA replication was increased (approximately 1.3-fold) after treatment with adriamycin (Fig. 3B), suggesting that the DNA damage response activates HCV RNA replication.

Suppression of HCV RNA replication by a small-molecule inhibitor of the ATM kinase. We next examined the effect of a specific small-molecule inhibitor of the ATM kinase (2-morpholin-4-yl-6-thianthren-1-yl-pyran-4-one [KU-55933]) (16) on HCV RNA replication. As expected, the ATM kinase inhibitor effectively inhibited Chk2 phosphorylation after adriamycin treatment in both sO and O cells (Fig. 3C). In this context, the ATM kinase inhibitor could efficiently suppress genome-length HCV RNA replication with an in vitro 50% effective concentration (EC_{50}) of approximately 2 μM at 72 h after treatment with adriamycin (Fig. 4A). Although this ATM kinase inhibitor did not affect cell viability at 24 h after the treatment, there was a slight decrease in the cell viability at 72 h after treatment (Fig. 4B). Thus, this or other ATM kinase inhibitors may be

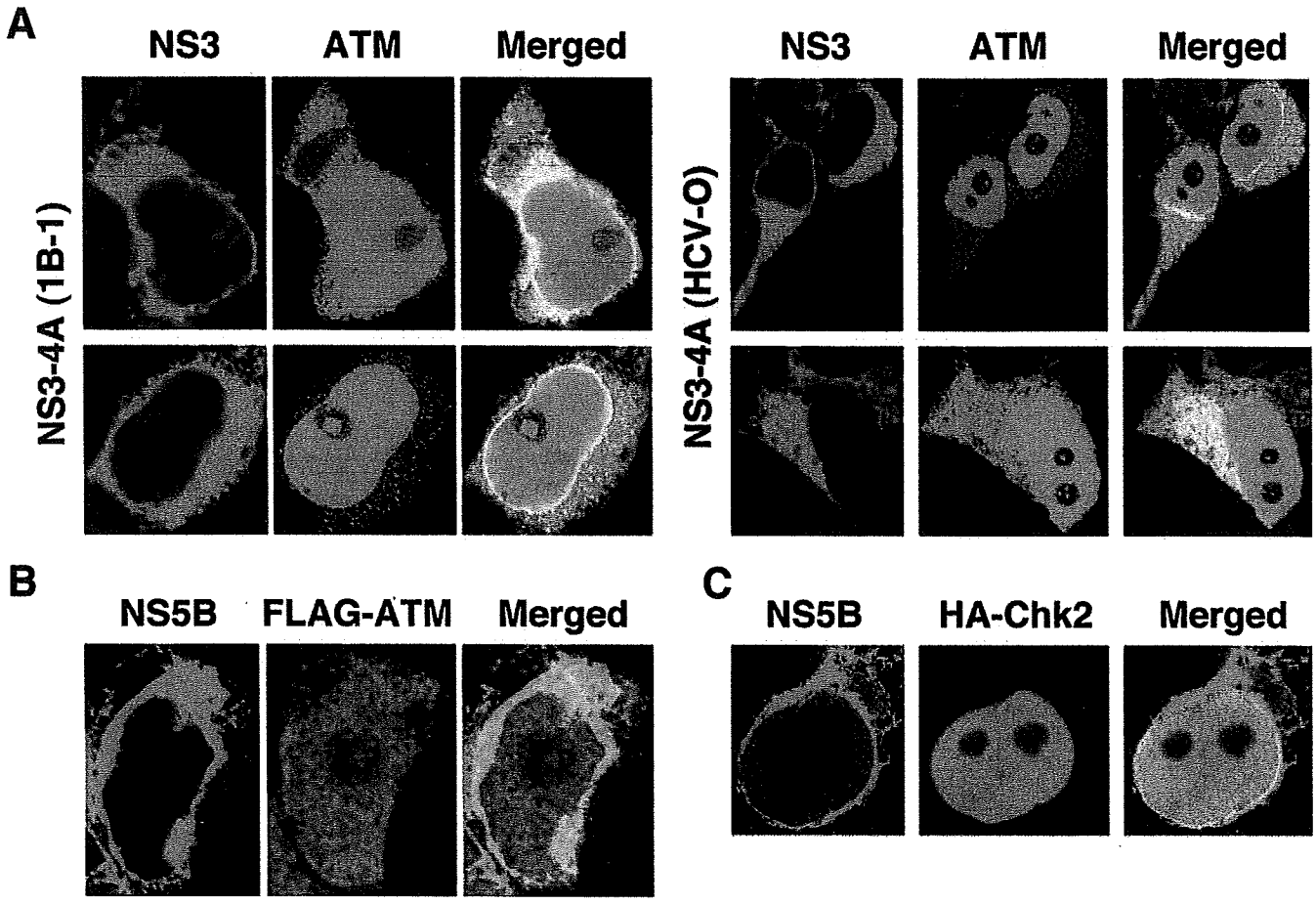

FIG. 5. Subcellular localization of ATM and Chk2 in HCV NS3-4A- or NS5B-expressing cells. (A) ATM partially colocalized with HCV NS3-4A. 293FT cells cotransfected with 300 ng of pCX4bsr/NS3-4A (1B-1) (8) or pCX4bsr/NS3-4A (O) (8) and 300 ng of pcDNA3-FLAG-ATMwt (6) were examined by confocal laser scanning microscopy. Cells were stained with anti-NS3 and anti-ATM (5C2) antibodies and then visualized with FITC (NS3) or Cy3 (ATM). (B) ATM partially colocalized with HCV NS5B. 293FT cells cotransfected with 300 ng of pCX4bsr/NS5B (1B-1) (23) and 300 ng of pcDNA3-FLAG-ATMwt (6). Cells were stained with anti-NS5B (no. 14) and anti-ATM (PM026) antibodies and then visualized with FITC (ATM) or Cy3 (NS5B). (C) Chk2 partially colocalized with HCV NS5B. 293FT cells cotransfected with 300 ng of pCX4bsr/NS5B (1B-1) (23) and 300 ng of pcDNA3-HA-Chk2wt (20, 21). Cells were stained with anti-NS5B and anti-HA (3F10) antibodies and then visualized with FITC (HA-Chk2) or Cy3 (NS5B). Images were visualized using confocal laser scanning microscopy (LSM510; Carl Zeiss). The right panels exhibit two-color overlay images (Merged). Colocalization is shown in yellow.

useful for the clinical treatment of patients with chronic hepatitis C.

Interaction of HCV NS3-4A with ATM. Since HCV NS3 has been proposed to be a viral factor involved in the induction of dsDNA breaks (18, 19), we first examined the subcellular localization of NS3-NS4A ([NS3-4A] 1B-1 or HCV-O strain) and ATM by confocal laser scanning microscopy. In most of the observed cells, ATM partially colocalized with NS3-4A in the perinuclear region and in dispersed points throughout the cytoplasm (Fig. 5A). In particular, we observed prominent colocalization of ATM with NS3-4A in some cells (Fig. 5A). Next, using anti-FLAG and anti-ATM antibodies, we immunoprecipitated lysates from 293FT cells in which FLAG-tagged ATM and either NS3-4A (HCV-O) or NS3 (HCV-O) were overexpressed and then performed immunoblotting analysis using either anti-ATM or anti-NS3 antibody to determine whether ATM binds to NS3-4A or NS3. The results revealed that ATM preferentially bound to NS3-4A over NS3 alone (Fig. 6A). Similarly, we found that ATM bound to NS3-4A using the O cell lysates (Fig. 6B), while HA-tagged Chk2 did not bind to NS3-4A in immunoprecipitation analysis using lysates from 293FT cells in which NS3-4A and HA-tagged Chk2 were overexpressed (Fig. 6C). Although NS3-4A has protease activity, ATM was not cleaved by the NS3-4A protease (Fig. 6D). Taking these results together, we conclude that ATM is able to interact with NS3-4A.

Interaction of HCV NS5B with ATM and Chk2. We next examined the subcellular localization of ATM and/or Chk2 in HCV NS5B-expressing cells by confocal laser scanning microscopy since we previously demonstrated that HCV NS5B-expressing PH5CH8 immortalized human hepatocyte cells were susceptible to DNA damage in the form of dsDNA breaks (23). ATM partially colocalized with NS5B in dispersed points throughout the cytoplasm (Fig. 5B), similar to the subcellular localization of HCV NS3-4A and ATM. Furthermore, Chk2 also partially colocalized with NS5B in the perinuclear region and in dispersed points in the nucleus (Fig. 5C). To determine whether endogenous ATM binds to NS5B, lysates from Oc or

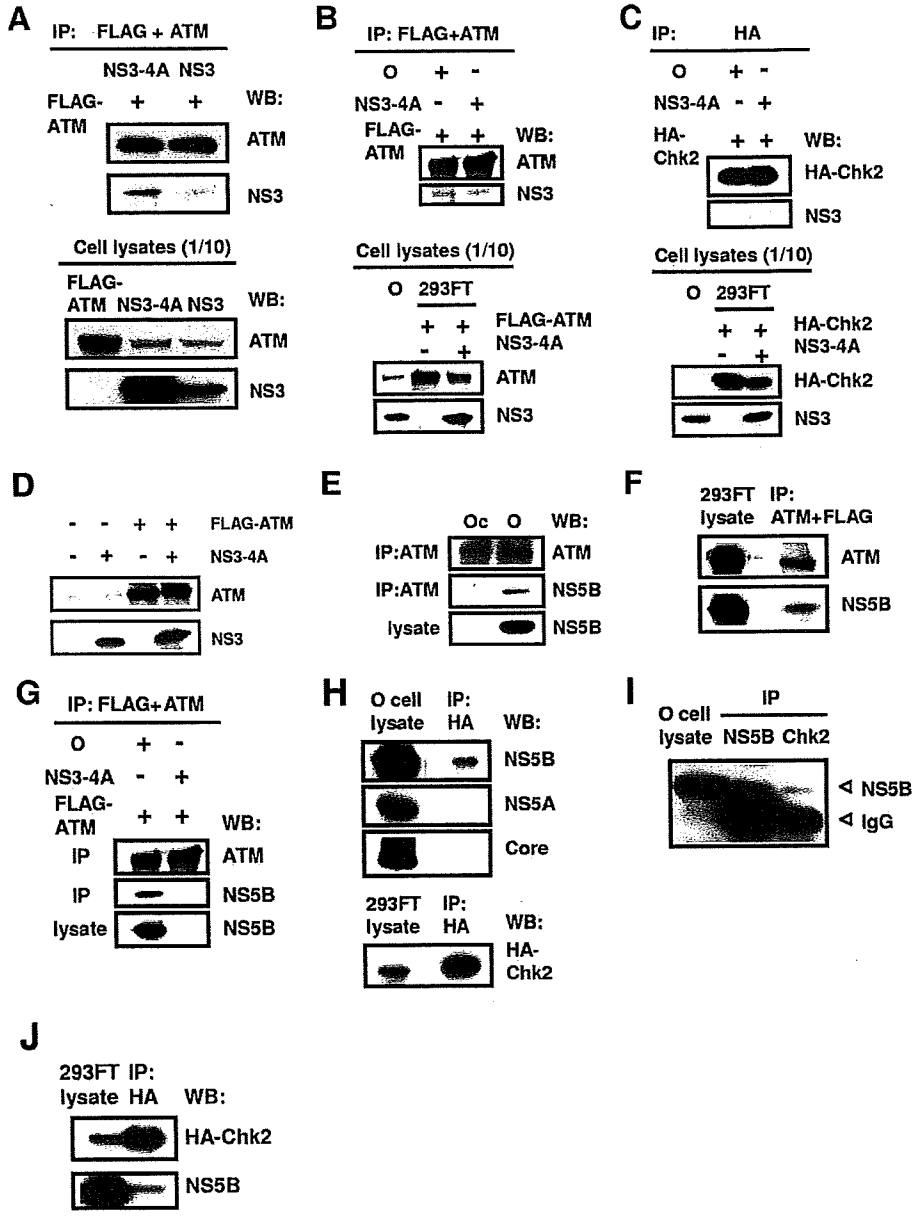

FIG. 6. Interaction of HCV NS3-4A and NS5B with the ATM signaling pathway. (A and B) ATM bound to HCV NS3-4A. (A) 293FT cells were transfected with 4 μg of pCX4bsr/NS3-4A (O), 4 μg of pCX4bsr/NS3 (O), or 4 μg of pcDNA3-FLAG-ATMwt. The cell lysates of expressed FLAG-ATM were mixed with lysates expressing either NS3-4A or NS3. The cell lysates were immunoprecipitated with both anti-FLAG (M2) and anti-ATM (2C1) antibodies, followed by immunoblotting analysis using either anti-ATM (2C1) or anti-HCV NS3 antibody. The results of Western blot analysis of 1/10 of the cellular lysates with anti-ATM or anti-NS3 antibody are also shown. (B) 293FT cells were cotransfected with 4 μg of pcDNA3-FLAG-ATMwt and/or 4 μg of pCX4bsr/NS3-4A (O). The cell lysates of expressed FLAG-ATM alone were mixed with the O cell lysates. Immunoprecipitation and Western blot analysis were performed as described in panel A. (C) Chk2 did not bind to NS3-4A. 293FT cells were cotransfected with 4 μg of pcDNA3-HA-Chk2wt and/or 4 μg of pCX4bsr/NS3-4A (O). The cell lysates of expressed HA-Chk2 alone were mixed with the O cell lysates. The cell lysates were immunoprecipitated with anti-HA antibody (3F10), followed by Western blot analysis using either anti-HA (HA-7) or anti-HCV NS3 antibody. The results of Western blot analysis of 1/10 of the cellular lysates with anti-HA or anti-NS3 antibody are also shown. (D) ATM was not cleaved by HCV NS3-4A protease. 293FT cells were cotransfected with 4 μg of pCX4bsr/NS3-4A (O) and/or 4 μg of pcDNA3-FLAG-ATMwt. The results of Western blot analysis of cellular lysates with anti-ATM or anti-NS3 antibody are shown. (E to G) ATM bound to HCV NS5B. (E) The lysates of O or Oc cells were immunoprecipitated with anti-ATM antibody (2C1), followed by immunoblotting analysis using either anti-ATM or anti-HCV NS5B antibody (no. 14). The results of Western blot analysis of 1/10 of the cellular lysates with anti-NS5B antibody are also shown. (F) 293FT cells were cotransfected with 4 μg of pCX4bsr/NS5B (1B-1) and 4 μg of pcDNA3-FLAG-ATMwt. The cell lysates were immunoprecipitated with both anti-FLAG and anti-ATM antibodies, followed by immunoblotting analysis using either anti-ATM or anti-HCV NS5B antibody. (G) Western Blot analysis was performed with anti-NS5B antibody, reusing the same blotted membrane that was used for panel B. (H to J) Chk2 bound to HCV NS5B. (H) 293FT cells were cotransfected with 4 μg of pcDNA3-HA-Chk2wt. The cell lysates of expressed HA-Chk2 were mixed with the O cell lysates and were immunoprecipitated with anti-HA antibody (3F10), followed by immunoblotting analysis using anti-HCV NS5B, anti-HCV NS5A (no. 8926), anti-HCV core protein (CP-9 and CP-11 mixture), or anti-HA (HA-7) antibody. The results of Western blot analysis of 1/10 of the cellular lysates with the same antibodies are also shown. (I) The lysates of O cells were immunoprecipitated with anti-NS5B or anti-Chk2 antibody (DCS-273), followed by immunoblotting analysis using anti-HCV NS5B antibody. The result of Western blot analysis of 1/10 of the cellular lysates with anti-NS5B antibody is also shown. (J) 293FT cells were cotransfected with 4 μg of pCX4bsr/NS5B (1B-1) and 4 μg of pcDNA3-HA-Chk2wt. The cell lysates were immunoprecipitated with anti-HA antibody (3F10), followed by immunoblotting analysis using either anti-HA (HA-7) or anti-HCV NS5B antibody. IP, immunoprecipitation; WB, Western blotting; IgG, immunoglobulin G.

O cells were immunoprecipitated with anti-ATM antibody, and then immunoblotting analysis using either anti-ATM or anti-NS5B antibody was performed. The results revealed that endogenous ATM bound to endogenous NS5B (Fig. 6E). Furthermore, we confirmed that ATM bound to NS5B in immunoprecipitation analysis using lysates from 293FT cells, in which NS5B (1B-1 strain) and FLAG-tagged ATM were overexpressed (Fig. 6F). Similarly, we confirmed that FLAG-tagged ATM bound to NS5B derived from O cell lysates in immunoprecipitation analysis using lysates from 293FT cells in which FLAG-tagged ATM was overexpressed (Fig. 6G). Finally, to determine which HCV protein binds to Chk2, the 293FT cell lysates of overexpressed HA-Chk2 were mixed with the O cell lysates and were immunoprecipitated with anti-HA antibody, followed by Western blot analysis using anti-HCV NS5B, anti-HCV NS5A, anti-HCV core protein, or anti-HA antibody. Consistent with the immunofluorescence result that Chk2 partially colocalized with NS5B (Fig. 5C), we observed that HA-tagged Chk2 bound to NS5B (Fig. 6H). Importantly, we found that endogenous Chk2 bound to endogenous NS5B derived from O cells (Fig. 6I). In addition, HA-tagged Chk2 bound to NS5B in immunoprecipitation analysis using lysates from 293FT cells in which NS5B (1B-1 strain) and HA-tagged Chk2 were overexpressed (Fig. 6J). Thus, Chk2 also interacted with NS5B as well as ATM. Taking these results together, we conclude that HCV targets ATM and Chk2 DNA damage sensors and that the ATM signaling pathway is required for HCV RNA replication.

DISCUSSION

ATM has been implicated as a target of most DNA viruses, harboring their genomes in the form of dsDNA which can activate or inhibit the ATM signaling pathway (17). In this study, we have demonstrated for the first time that the ATM signaling pathway is required for HCV RNA replication even though HCV does not have a dsDNA genome, unlike DNA viruses. In this regard, Machida et al. previously proposed that HCV infection and the expression of HCV NS3 and core protein induced dsDNA breaks (18, 19). Furthermore, NS3 has DNA helicase activity by which it unwinds dsDNA, suggesting that NS3 affects host dsDNA (22, 25). Thus, HCV infection might trigger the activation of ATM without a dsDNA genome. In fact, we observed weak but significant phosphorylation of Chk2 at threonine 68, the specific marker for ATM activation, in the HCV RNA-replicating cells (O and sO cells) but not in the HCV-negative Oc and sOc cells (Fig. 3A), suggesting that the ATM-dependent DNA damage response is constantly stimulated in persistent HCV RNA-replicating cells. Furthermore, we demonstrated that ATM preferentially bound to NS3-4A over NS3 alone (Fig. 5B) and that ATM partially colocalized with NS3-4A in the perinuclear region, where HCV is known to form a replication complex and replicate itself, and in dispersed points throughout the cytoplasm (Fig. 5A), indicating the interaction of ATM with NS3-4A. Interestingly, Lai et al. very recently reported that NS3-4A impaired DNA repair and enhanced sensitivity to ionizing radiation through interaction with ATM (15). However, we observed an equivalent level of Chk2 phosphorylation at threonine 68, a direct downstream target of ATM (20, 21), in both HCV RNA-replicating cells (O cells) and HCV-negative cells (Oc cells) after treatment with adriamycin (Fig. 3A), suggesting that Chk2 phosphorylation by ATM is not impaired by HCV RNA replication. In this regard, Gaspar and Shenk also showed that human cytomegalovirus could inhibit a DNA damage response by mislocalizing ATM and phosphorylated Chk2 at threonine 68 to a cytoplasmic virus assembly zone, indicating that human cytomegalovirus blocked at the level of Chk2 (9). On the other hand, dsDNA triggers IFN immune defenses through retinoic acid-induced gene I, the mitochondrial antiviral signaling protein, or the DNA-dependent activator of IFN-regulatory factor (7, 26); and NS3-4A protease, which is known to cleave the mitochondrial antiviral signaling protein, can block it (26), suggesting that interaction of NS3-4A with ATM is partially involved in such a common antiviral signaling pathway. On the other hand, we previously demonstrated that HCV NS5B-expressing PH5CH8 immortalized human hepatocyte cells were susceptible to DNA damage in the form of dsDNA breaks (23). In this regard, we have found that HCV NS5B could bind to both ATM and Chk2 (Fig. 5B and C and 6E to J). Together, these results indicate that HCV might hijack ATM and Chk2 and utilize ATM and Chk2 for HCV RNA replication, thereby resulting in impairment of DNA repair, enhancement of mutation frequency, and development of hepatocellular carcinoma.

Finally, consistent with our finding that ATM was required for HCV RNA replication, an ATM kinase inhibitor efficiently suppressed genome-length HCV RNA replication at an EC_{50} of approximately 2 μM at 72 h after the treatment (Fig. 4A). Similarly, Lau et al. reported that the same ATM kinase inhibitor could suppress HIV-1 replication at an EC_{50} of approximately 2.3 μM (16). Importantly, the EC_{50} for HIV-1 replication is similar to that for HCV replication. Thus, this or other ATM kinase inhibitors may represent a novel approach for the clinical treatment of patients with chronic hepatitis C as well as AIDS patients.

ACKNOWLEDGMENTS

We thank D. Trono, R. Agami, R. Iggo, M. Kastan, S. J. Elledge, M. Kohara, A. Takamizawa, and M. Hijikata for the VSV-G-pseudotyped HIV-1-based vector system (pCMVR8.91 and pMDG2) and for pSUPER, pRDI292, pcDNA3-FLAG-ATM, and pcDNA3-HA-Chk2, and for anti-NS3 antibody, anti-NS5B antibody, anti-NS5A antibody, and 293FT cells. We also thank A. Morishita and T. Nakamura for their technical assistance.

This work was supported by a Grant-in-Aid for Young Scientists (B) from the Ministry of Education, Culture, Sports, Science and Technology (MEXT); by a Grant-in-Aid for Research on Hepatitis from the Ministry of Health, Labor, and Welfare of Japan; by the Ichiro Kanehara Foundation; and by a Research Fellowship from the Japan Society for the Promotion of Science.

REFERENCES

1. **Ariumi, Y., P. Turelli, M. Masutani, and D. Trono.** 2005. DNA damage sensors ATM, ATR, DNA-PKcs, and PARP-1 are dispensable for human immunodeficiency virus type 1 integration. J. Virol. **79**:2973–2978.
2. **Ariumi, Y., and D. Trono.** 2006. Ataxia-telangiectasia-mutated (ATM) protein can enhance human immunodeficiency virus type 1 replication by stimulating Rev. function. J. Virol. **80**:2445–2452.
3. **Ariumi, Y., M. Kuroki, K. Abe, H. Dansako, M. Ikeda, T. Wakita, and N. Kato.** 2007. DDX3 DEAD-box RNA helicase is required for hepatitis C virus RNA replication. J. Virol. **81**:13922–13926.
4. **Bridge, A. J., S. Pebernard, A. Ducraux, A.-L. Nicoulaz, and R. Iggo.** 2003. Induction of an interferon response by RNAi vectors in mammalian cells. Nat. Genet. **34**:263–264.

5. **Brummelkamp, T. R., R. Bernard, and R. Agami.** 2002. A system for stable expression of short interfering RNAs in mammalian cells. Science **296:**550–553.
6. **Canman, C. E., D.-S. Lim, K. A. Cimprich, Y. Taya, K. Tamai, K. Sakaguchi, E. Apella, M. B. Kastan, and J. D. Siliciano.** 1998. Activation of the ATM kinase by ionizing radiation and phosphorylation of p53. Science **281:**1677–1679.
7. **Cheng, G., J. Zhong, J. Chung, and F. V. Chisari.** 2007. Double-stranded DNA and double-stranded RNA induces a common antiviral signaling pathway in human cells. Proc. Natl. Acad. Sci. USA **104:**9035–9040.
8. **Dansako, H., M. Ikeda, and N. Kato.** 2007. Limited suppression of the interferon-beta production by hepatitis C virus serine protease in cultured human hepatocytes. FEBS J. **274:**4161–4176.
9. **Gaspar, M., and T. Shenk.** 2006. Human cytomegalovirus inhibits a DNA damage response by mislocalizing checkpoint proteins. Proc. Natl. Acad. Sci. USA **103:**2821–2826.
10. **Harper, J. W., and S. J. Elledge.** 2007. The DNA damage response: ten years after. Mol. Cell **28:**739–745.
11. **Ikeda, M., K. Abe, H. Dansako, T. Nakamura, K. Naka, and N. Kato.** 2005. Efficient replication of a full-length hepatitis C virus genome, strain O, in cell culture, and development of a luciferase reporter system. Biochem. Biophys. Res. Commun. **329:**1350–1359.
12. **Kato, N., M. Hijikata, Y. Ootsuyama, M. Nakagawa, S. Ohkoshi, T. Sugimura, and K. Shimotohno.** 1990. Molecular cloning of the human hepatitis C virus genome from Japanese patients with non-A, non-B hepatitis. Proc. Natl. Acad. Sci. USA **87:**9524–9528.
13. **Kato, N.** 2001. Molecular virology of hepatitis C virus. Acta Med. Okayama **55:**133–159.
14. **Kato, N., K. Sugiyama, K. Namba, H. Dansako, T. Nakamura, M. Takami, K. Naka, A. Nozaki, and K. Shimotohno.** 2003. Establishment of a hepatitis C virus subgenomic replicon derived from human hepatocytes infected in vitro. Biochem. Biophys. Res. Commun. **306:**756–766.
15. **Lai, C. K., K. S. Jeng, K. Machida, Y. S. Cheng, and M. M. Lai.** 2008. Hepatitis C virus NS3/4A protein interacts with ATM, impairs DNA repair and enhances sensitivity to ionizing radiation. Virology **370:**295–309.
16. **Lau, A., K. M. Swinbank, P. S. Ahmed, D. L. Taylor, S. P. Jackson, G. C. Smith, and M. J. O'Connor.** 2005. Suppression of HIV-1 infection by a small molecule inhibitor of the ATM kinase. Nat. Cell Biol. **7:**493–500.
17. **Lilley, C. E., R. A. Schwartz, and M. D. Weitzman.** 2007. Using or abusing: viruses and the cellular DNA damage response. Trends Microbiol. **15:**119–126.
18. **Machida, K., K. T. Cheng, V. M. Sung, S. Shimodaira, K. L. Lindsay, A. M. Levine, M. Y. Lai, and M. M. Lai.** 2004. Hepatitis C virus induces a mutator phenotype: enhanced mutations of immunoglobulin and protooncogenes. Proc. Natl. Acad. Sci. USA **101:**4262–4267.
19. **Machida, K., K. T. Cheng, V. M. Sung, K. J. Lee, A. M. Levine, and M. M. Lai.** 2004. Hepatitis C virus infection activates the immunologic (type II) isoform of nitric oxide synthase and thereby enhances DNA damage and mutations of cellular genes. J. Virol. **78:**8835–8843.
20. **Matsuoka, S., M. Huang, and S. J. Elledge.** 1998. Linkage of ATM to cell cycle regulation by the Chk2 protein kinase. Science **282:**1893–1897.
21. **Matsuoka, S., G. Rotman, A. Ogawa, Y. Shiloh, K. Tamai, and S. J. Elledge.** 2000. Ataxia telangiectasia-mutated phosphorylates Chk2 in vivo and in vitro. Proc. Natl. Acad. Sci. USA **97:**10389–10394.
22. **Myong, S., M. M. Bruno, A. M. Pyle, and T. Ha.** 2007. Spring-loaded mechanism of DNA unwinding by hepatitis C virus NS3 helicase. Science **317:**513–516.
23. **Naka, K., H. Dansako, N. Kobayashi, M. Ikeda, and N. Kato.** 2006. Hepatitis C virus NS5B delays cell cycle progression by inducing interferon-β via Toll-like receptor 3 signaling pathway without replicating viral genomes. Virology **346:**348–362.
24. **Naldini, L., U. Blömer, P. Gallay, D. Ory, R. Mulligan, F. H. Gage, I. M. Verma, and D. Trono.** 1996. In vivo gene delivery and stable transduction of nondividing cells by a lentiviral vector. Science **272:**263–267.
25. **Pang, P. S., E. Jankowsky, P. J. Planet, and A. M. Pyle.** 2002. The hepatitis C viral NS3 protein is a processive DNA helicase with cofactor enhanced RNA unwinding. EMBO J. **21:**1168–1176.
26. **Takaoka, A., Z. Wang, M. K. Choi, H. Yanai, H. Negishi, T. Ban, Y. Lu, M. Miyagishi, T. Kodama, K. Honda, Y. Ohba, and T. Taniguchi.** 2007. DAI (DLM-1/ZBP1) is a cytosolic DNA sensor and an activator of innate immune response. Nature **448:**501–505.
27. **Tanaka, T., N. Kato, M. J. Cho, and K. Shimotohno.** 1995. A novel sequence found at the 3′ terminus of hepatitis C virus genome. Biochem. Biophys. Res. Commun. **215:**744–749.
28. **Thomas, D. L.** 2000. Hepatitis C epidemiology. Curr. Top. Microbiol. Immunol. **242:**25–41.
29. **Wakita, T., T. Pietschmann, T. Kato, T. Date, M. Miyamoto, Z. Zhao, K. Murthy, A. Habermann, H. G. Kräusslich, M. Mizokami, R. Bartenschlager, and T. J. Liang.** 2005. Production of infectious hepatitis C virus in tissue culture from a cloned viral genome. Nat. Med. **11:**791–796.
30. **Zufferey, R., D. Nagy, R. J. Mandel, L. Naldini, and D. Trono.** 1997. Multiply attenuated lentiviral vector achieves efficient gene delivery in vivo. Nat. Biotechnol. **15:**871–875.

Biochemical and Biophysical Research Communications 371 (2008) 104–109

Contents lists available at ScienceDirect

Biochemical and Biophysical Research Communications

journal homepage: www.elsevier.com/locate/ybbrc

New efficient replication system with hepatitis C virus genome derived from a patient with acute hepatitis C ☆

Kyoko Mori, Ken-ichi Abe, Hiromichi Dansako, Yasuo Ariumi, Masanori Ikeda, Nobuyuki Kato *

Department of Molecular Biology, Okayama University Graduate School of Medicine, Dentistry, and Pharmaceutical Sciences, 2-5-1 Shikata-cho, Okayama 700-8558, Japan

ARTICLE INFO

Article history:
Received 25 March 2008
Available online 10 April 2008

Keywords:
Hepatitis C virus
Acute hepatitis C
HCV replication system
Genome-length HCV RNA
Anti-HCV reagents
Interferon-γ

ABSTRACT

We report for the first time a new RNA replication system with a hepatitis C virus (HCV) strain (AH1) derived from a patient with acute hepatitis C. Using an HCV replicon RNA library constructed with the AH1 strain (genotype 1b), we first established a cloned cell line, sAH1, harboring the HCV replicon. Cured cells obtained with interferon treatment of sAH1 cells were used for transfection with genome-length HCV RNA possessing four mutations found in sAH1 replicon. Consequently, one cloned cell line, AH1, supporting efficient replication of genome-length HCV RNA was obtained. By the comparison of AH1 cells with the O cells supporting genome-length HCV RNA (HCV-O strain) replication, we found different anti-HCV profiles of interferon-γ and cyclosporine A between AH1 and O cells. Reporter assay analysis suggests that the diverse effects of interferon-γ are due to the difference in HCV strains, but not the cellular environment.

Hepatitis C virus (HCV) infection frequently causes chronic hepatitis, which progresses to liver cirrhosis and hepatocellular carcinoma. HCV infection has now become a serious health problem because at least 170 million people worldwide are currently infected with HCV [1]. HCV is an enveloped virus with a positive single-stranded 9.6 kilobase (kb) RNA genome, which encodes a large polyprotein precursor of approximately 3000 amino acid (aa) residues [2,3]. This polyprotein is cleaved by a combination of the host and viral proteases into at least 10 proteins in the following order: core, envelope 1 (E1), E2, p7, non-structural 2 (NS2), NS3, NS4A, NS4B, NS5A, and NS5B [3].

As a striking breakthrough in HCV research, in 1999, an HCV replicon system enabling robust HCV subgenomic RNA (Con-1 strain of genotype 1b) replication in specific human HuH-7 hepatoma cells has been developed [4]. After the first Con-1 replicon, several HCV replicon (genotypes 1a, 1b, and 2a) systems using HuH-7-derived cells have been developed. These replicon systems have become powerful tools for basic studies of HCV replication, HCV–host cell interactions, and screening of anti-HCV reagents, [5,6]. Furthermore, genome-length HCV RNA replication systems have been developed [7–9], since HCV replicons lacking HCV structural proteins are insufficient for further HCV research. We also established a genome-length HCV RNA-replicating cell line (HCV-O strain of genotype 1b; called O cell line) [10] using cured cells derived from sO cells [11], in which HCV replicon RNA (HCV-O strain) with an adaptive mutation (S2200R) is replicating. However, to date, established genome-length HCV RNA-replicating stable cell lines are limited to five HCV strains, H77 (1a), HCV-N (1b), Con-1 (1b), HCV-O (1b), and JFH1 (2a) [7–10,12], and there is no RNA replication system with an HCV strain derived from a patient with acute hepatitis C. Furthermore, there have been few reports comparing these HCV strains.

To clarify these problems, we have attempted to establish a new stable cell line, in which genome-length HCV RNA derived from a patient with acute hepatitis C is efficiently replicating. We report herein a new efficient RNA replication system with HCV derived from a patient with acute hepatitis C and provide a comparative analysis of RNA replication systems with AH1 and HCV-O strains regarding the sensitivities to anti-HCV reagents, including interferon (IFN)-α.

Materials and methods

Cell culture. Cells supporting HCV replicon or genome-length HCV RNA, and cured cells, from which the HCV RNA had been eliminated by IFN treatment, were maintained as described previously [10].

Reverse transcription (RT)-nested PCR. RNA from a serum of patient AH1 [13] with acute hepatitis C was prepared using the ISOGEN-LS extraction kit (Nippon Gene Co., Japan). This RNA sample was used as a template for RT-nested PCR to amplify the HCV RNA. RT-nested PCR was performed separately in two parts; one part (3.5 kb) covered from HCV 5′UTR to NS3, and the other part (6 kb) covered from NS2 to NS5B. For the first part, the antisense primer AH3553R, 5′-CACACGCCGTTGATGC AGGTCG-3′ was used for RT. Primers 21 [11] and AH3519R, 5′-TGCGTGGCGG

☆ The nucleotide sequence data reported in this paper will appear in the DDBJ, EMBL, and GenBank nucleotide sequence databases under Accession No. AB429050.

* Corresponding author. Fax: +81 86 235 7392.
E-mail address: nkato@md.okayama-u.ac.jp (N. Kato).

0006-291X/$ - see front matter © 2008 Elsevier Inc. All rights reserved.
doi:10.1016/j.bbrc.2008.04.005

TGGAAACCACCTG-3′ were employed in the first round of PCR (35 cycles). An internal primer pair (21X [11] and AH3466RX: 5′-ATTATTCTAGAGGCCTGTGAGACTG GTGATGATGC-3′; containing a XbaI site (underlined)) was used for the second round of PCR (35 cycles). For the second part, the antisense primer 386R [11] was used for RT. Primers 542 and 9388R [11] were employed in the first round of PCR (35 cycles). An internal primer pair (3295X: 5′-ATTATTCTAGACTGACATGGA GACCAAGATCATCAC-3′; containing a XbaI site (underlined) and 9357RX: 5′-ATTATT CTAGACCCGTTCACCGGTTGGGGAGCAG-3′; containing a XbaI site (underlined)) was used for the second round of PCR (35 cycles). These fragments overlapped at the NS2 and NS3 regions and were used for sequence analysis for HCV RNA after cloning into the XbaI site of pBR322MC [11]. Superscript II (Invitrogen) and KOD-plus DNA polymerase (Toyobo, Osaka, Japan) were used for RT and PCR, respectively.

Plasmid construction. PCR product (NS3 to NS5B of AH1 strain) with primers 542 and 9388R was further amplified with primers 3501S: 5′-ATTATACTAGTCTCACAGG CCGGGACAAGAACC-3′; containing a SpeI site (underlined) and 9162RB: 5′-ATTATC GTACGGCCCAGTTGAAGAGGTACTTGCC-3′; containing a BsiWI site (underlined). The amplified fragment was digested with SpeI and BsiWI, and ligated into the replicon cassette plasmid pNSS1RZ2RU [11], which was predigested with SpeI and BsiWI. Using this ligation reaction mixture, a replicon RNA library (AH1N/3-5B in Supplementary Fig. 1) was prepared by a previously described method [11]. To make the plasmid pAH1N/C-5B/PL, LS, $(VA)_2$ containing full-length HCV polyprotein of AH1 strain, pON/C-5B containing full-length HCV polyprotein of HCV-O strain [10] was utilized. First, to make a fragment for pAH1N/C-5B (Supplementary Fig. 1), overlapping PCR was used to fuse EMCV IRES to the core protein-coding sequence of the AH1 strain, as described previously [10]. The resulting DNA was digested with PmeI and ClaI, and then replaced with the PmeI–ClaI fragment of pON/C-5B (pON/C-5B/CoreAH was obtained). Second, the ClaI–AgeI fragment of pHCV-AH1 containing full-length HCV polyprotein of AH1 strain was replaced with the ClaI–AgeI fragment of pON/C-5B/CoreAH (pAH1N/C-5B was obtained). Finally, the SpeI–BsiWI fragment of pAH1N/3-5B clone 2 (see Fig. 1C) was replaced with the SpeI–BsiWI fragment of pAH1N/C-5B (pAH1N/C-5B/PL, LS, $(VA)_2$ was obtained).

RNA synthesis. Plasmid DNAs were linearized by XbaI and were used for RNA synthesis with T7 MEGAscript (Ambion) as previously described [11].

RNA transfection and selection of G418-resistant cells. The transfection of HCV replicon RNA or genome-length HCV RNA synthesized in vitro into HuH-7-derived cells was performed by electroporation, and the cells were selected in the presence of G418 (0.3 mg/ml; Promega) for 3 weeks as described previously [11].

Quantification of HCV RNA. The quantitative RT-PCR (RT-qPCR) analysis for HCV RNA was performed by LightCycler PCR as described previously [10]. Experiments were done in triplicate.

Integration analysis. Genomic DNA was extracted from the cultured cells using the DNeasy Blood & Tissue Kit (QIAGEN). The HCV 5′UTR and the IFN-β gene were detected according to a PCR method described previously [11].

Western blot analysis. The preparation of cell lysates, sodium dodecyl sulfate–polyacrylamide gel electrophoresis, and immunoblotting analysis were performed as previously described [11]. The antibodies used in this study were those against Core, E2, NS3, NS4A, NS5A, and NS5B [10]. β-Actin antibody (AC-15, Sigma) was used as the control for the amount of protein loaded per lane. Immunocomplexes were detected with the Renaissance enhanced chemiluminescence assay (Perkin-Elmer Life Sciences, Boston, MA).

Sequence analysis of HCV RNA. To amplify replicon RNA and genome-length HCV RNA, RT-PCR was performed as described previously [10,11]. The PCR products were subcloned into the XbaI site of pBR322MC, and sequence analysis was performed as described previously [11].

Northern blot analysis. Total RNA was extracted from the cultured cells using the RNeasy Mini Kit (QIAGEN). Three micrograms of total RNA was used for the analysis. HCV-specific RNA and β-actin were detected according to a method described previously [10].

Luciferase reporter assay. For the dual-luciferase assay, firefly luciferase vectors, pGBP-1(-216)-Luc and p2′–5′-OAS(-159)-Luc [14], were used. The reporter assay was performed as previously described [14]. The experiments were performed in at least triplicate.

Statistical analysis. Differences between AH1 and O cell lines were tested using the Student's *t*-test. *P* values <.05 were considered statistically significant.

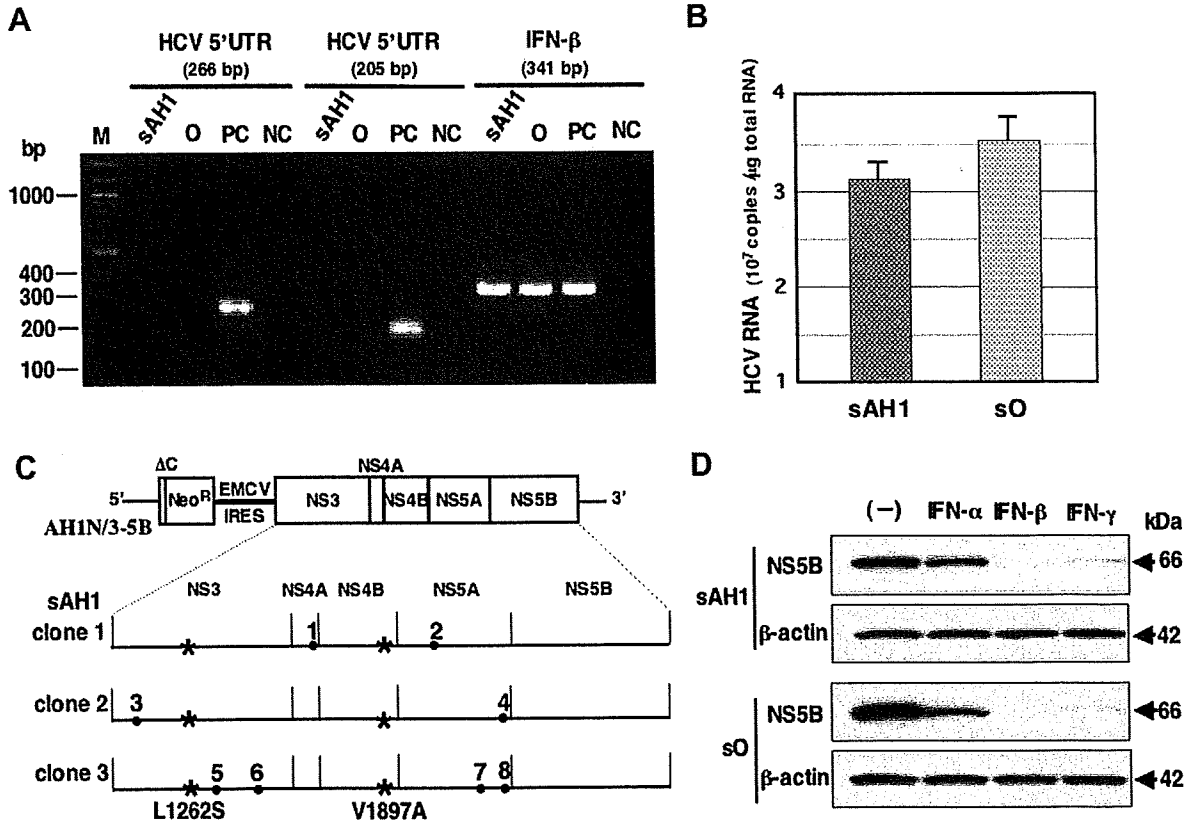

Fig. 1. Characterization of sAH1 cells harboring HCV replicon. (A) No integration of the HCV sequence in the genomic DNA. Genomic DNA from sAH1cells was subjected to PCR for the detection of the HCV 5′UTR and the IFN-β gene. O cells were used as a negative control. Lane PC, HCV sequence-integrated cells; lane NC, no genomic DNA; lane M, 100 bp DNA ladder. PCR products were detected by staining with ethidium bromide after 3% agarose gel electrophoresis. (B) Quantitative analysis of intracellular replicon RNA. The levels of replicon RNA were quantified by LightCycler PCR. sO cells harboring HCV-O replicon [11] were used for the comparison. (C) Amino acid substitutions detected in intracellular AH1 replicon RNA. NS3 to NS5B regions of three independent clones sequenced were presented. L1262S and V1897A conserved substitutions are indicated by asterisks. Clone-specific aa substitutions (indicated by the numbers with dots) are as follows: 1, K1691R; 2, M2105I; 3, P1115L; 4, V2360A; 5, K1368R; 6, A1533T; 7, I2285V; 8, D2377H. (D) IFN sensitivity of AH1 replicon. sAH1 cells were treated with IFN-α (Sigma), IFN-β (a gift from Toray Industries), and IFN-γ (Sigma) (20 IU/ml each) for 5 days. For the comparison, sO cells were treated as well as sAH1 cells. NS5B was detected by Western blot analysis.

Results

Establishment of a G418-resistant cell line (sAH1) harboring HCV replicon RNA

An HCV replicon RNA library prepared from the AH1 strain was first transfected into sOc cells (cured sO cells) [11], and the G418-resistant cells were selected as described previously [11]. Although several G418-resistant colonies were obtained, production of these colonies was due to integration of the HCV RNA sequence into the chromosomal DNA (PC in Fig. 1A). Therefore, we further cleaned up the replicon RNA library with additional DNase treatment, and it was then transfected into OR6c cells (cured OR6 cells) [10]. Consequently, a G418-resistant colony was obtained and successfully proliferated; this colony was referred to as sAH1. To exclude the possibility of integration of a replicon RNA sequence into the genomic DNA, we examined the presence of the HCV 5′UTR sequence in the genomic DNA isolated from sAH1 cells by a PCR method described previously [11]. Genome-length HCV RNA-replicating O cells were also examined as a negative control. The results revealed that the HCV RNA sequence was not integrated into the genomic DNA in either sAH1 cells or O cells (Fig. 1A).

Regarding the level of replicon RNA in sAH1 cells, RT-qPCR analysis revealed that the titer of replicon RNA was approximately 3×10^7 copies/μg total RNA, and its level was equivalent to that in sO cells (Fig. 1B), suggesting that the efficiency of RNA replication in sAH1 cells is similar to that in sO cells.

To exclude the possibility that sAH1 cells were derived from a small number of OR6 cells remaining after IFN treatment, and to determine whether replicon RNA in sAH1 cells possesses cell culture-adaptive mutations [5], which enhance the efficiency of RNA replication, we performed genetic analysis of the intracellular AH1 replicon. The sequences of three independent clones were determined and compared with each other to avoid PCR error. The obtained consensus nucleotide and aa sequences of NS3–NS5B regions of the AH1 replicon showed 7.3% and 3.7% differences, respectively, from those of the HCV-O replicon [11], indicating that sAH1 cells were not contaminated by the OR6 cells. In contrast, to find conserved mutations in the AH1 replicon, we determined the consensus nucleotide sequences of AH1 serum-derived HCV RNA by comparison of the nucleotide sequences of three independently isolated cDNA clones (Accession No. AB429050). The K1609E (NS3) and S2200R (NS5A) adaptive mutations found in O and OR6 cells were not detected in the AH1 replicon. However, instead of these mutations, L1262S (NS3) and V1897A (NS4B) conserved mutations were detected (Fig. 1C). Although V1897A has been detected as an adaptive mutation in Con-1 replicon [15], L1262S has until now remained undetected. In clone 2, the P1115L mutation (number 3 in Fig. 1C), which has been reported as an adaptive mutation [15,16], was detected.

To further characterize the sAH1 replicon, we compared the sensitivities of sAH1 and sO replicons against anti-HCV reagents (IFN-α, IFN-β, and IFN-γ) [5,6,11]. Western blot analysis of NS5B revealed that the IFN sensitivity of the sAH1 replicon was equivalent to that of the sO replicon (Fig. 1D).

Establishment of a genome-length HCV-AH1 RNA-replicating cell line, AH1

To develop a genome-length HCV RNA replication system, we first constructed a pAH1N/C-5B/PL, LS, $(VA)_2$ by the replacement with sAH1 replicon clone 2 (Fig. 1C) into pAH1N/C-5B. AH1N/C-5B/PL, LS, $(VA)_2$ RNA was transfected into sAH1c cells, cured sAH1 cells. Following 3 weeks of culturing in the presence of

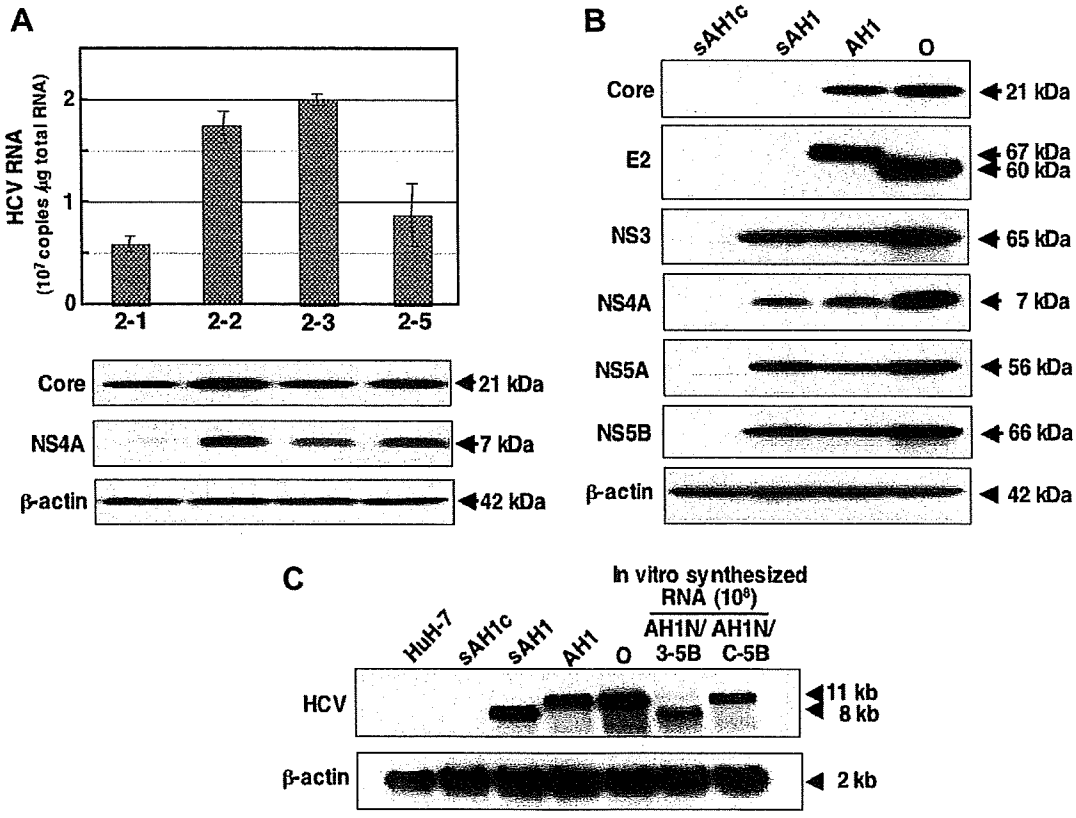

Fig. 2. Characterization of AH1 cells harboring genome-length HCV RNA. (A) Selection of G418-resistant cell lines. The levels of HCV RNA in G418-resistant cells were quantified by LightCycler PCR (upper panel). Core and NS4A were detected by Western blot analysis (lower panel). (B) Western blot analysis. AH1, O, sAH1, and sAH1c cells were used for the comparison. Core, E2, NS3, NS4A, NS5A, and NS5B were detected by Western blot analysis. (C) Northern blot analysis. AH1, O, sAH1, sAH1c, and HuH-7 cells were used for the comparison. In vitro-synthesized AH1N/3-5B and AH1N/C-5B RNAs were also used for the comparison.

G418, several colonies were obtained, and 4 colonies (2-1, 2-2, 2-3, and 2-5) then successfully proliferated. We selected colony 2-2 among them because it showed high levels of HCV RNA and proteins (core and NS4A) (Fig. 2A); this cell line was referred to as AH1. To compare the expression levels of HCV proteins in AH1 cells with those in O cells, Western blot analysis was further performed. Although the levels of HCV proteins in AH1 cells were slightly lower than those in O cells, the expression levels of NS proteins in AH1 cells were equivalent to those in sAH1 cells (Fig. 2B). In this analysis, we noticed that the size of the E2 protein in AH1 cells was 7 kDa larger than that in O cells (Fig. 2B). This difference may be due to the different numbers of *N*-glycosylation sites in E2 protein, since 11 and 9 *N*-glycosylation sites in E2 proteins are estimated in AH1 and HCV-O strains, respectively. Northern blot analysis also showed the presence of HCV-specific RNA with a length of approximately 11 kb in the extracts of total RNA prepared from AH1 cells, similar to that in the O cells (Fig. 2C). We confirmed the presence of replicon RNA (approximately 8 kb) in sAH1 cells (Fig. 2C). To check the additional adaptive mutations in the genome-length AH1 RNA, we performed sequence analysis of HCV RNA in AH1 cells. The results (Supplementary Fig. 2) revealed no additional mutations detected commonly among the three independent clones sequenced, suggesting that additional adaptive mutations are not required for genome-length HCV RNA replication. We therefore conclude that the AH1 cell line can be used as a genome-length HCV RNA replication system with acute hepatitis C-derived HCV strain.

Diverse effects of anti-HCV reagents on HCV RNA replication in AH1 and O cells

To compare the effects of anti-HCV reagents on RNA replication systems with different HCV strains, we examined the anti-HCV profiles of IFN-α, IFN-γ, and cyclosporine A (CsA) [17] using AH1 and O cells. Regarding IFN-α, the anti-HCV effect in AH1 cells was similar to that in O cells (Fig. 3A). Although RT-qPCR analysis showed a statistically significant difference in both cell systems when 1 IU/ml of IFN-α was used, such a difference was not observed in the Western blot analysis (Fig. 3A). In contrast, a significant different effect of IFN-γ was observed in both cell systems. RT-qPCR and Western blot analyses revealed that RNA replication of the AH1 strain was less sensitive than that of the HCV-O strain when 1 or 10 IU/ml of IFN-γ was used (Fig. 3B). Conversely, we observed that RNA replication of the AH1 strain was more sensitive to CsA than that of the HCV-O strain (Fig. 3C). These results suggest that anti-HCV profiles of IFN-γ and CsA are rather different between AH1 and O cell systems.

Different anti-HCV profile of IFN-γ is not correlated with the cellular potentials of the IFN-γ signaling pathway

To clarify whether the different effects of IFN-γ observed between AH1 and O cells are dependent on the cellular potentials of the IFN-γ signaling pathway, we performed a dual-luciferase reporter assay using an IFN-γ-inducible intrinsic GBP-1 gene promoter. As a control, IFN-α-inducible intrinsic 2′–5′-OAS gene promoter was also used for the analysis of the IFN-α signaling pathway. The results revealed that a good response of both AH1 and O cells to IFN-α and IFN-γ stimulation, with their potentials for both signaling pathways being almost the same (Fig. 4). These results suggest that the diverse anti-HCV effects of IFN-γ are dependent on the HCV strain, but not on the cellular potentials of the IFN-γ signaling pathway.

Discussion

In the present study, we established for the first time an HCV RNA replication system with AH1 strain derived from a patient

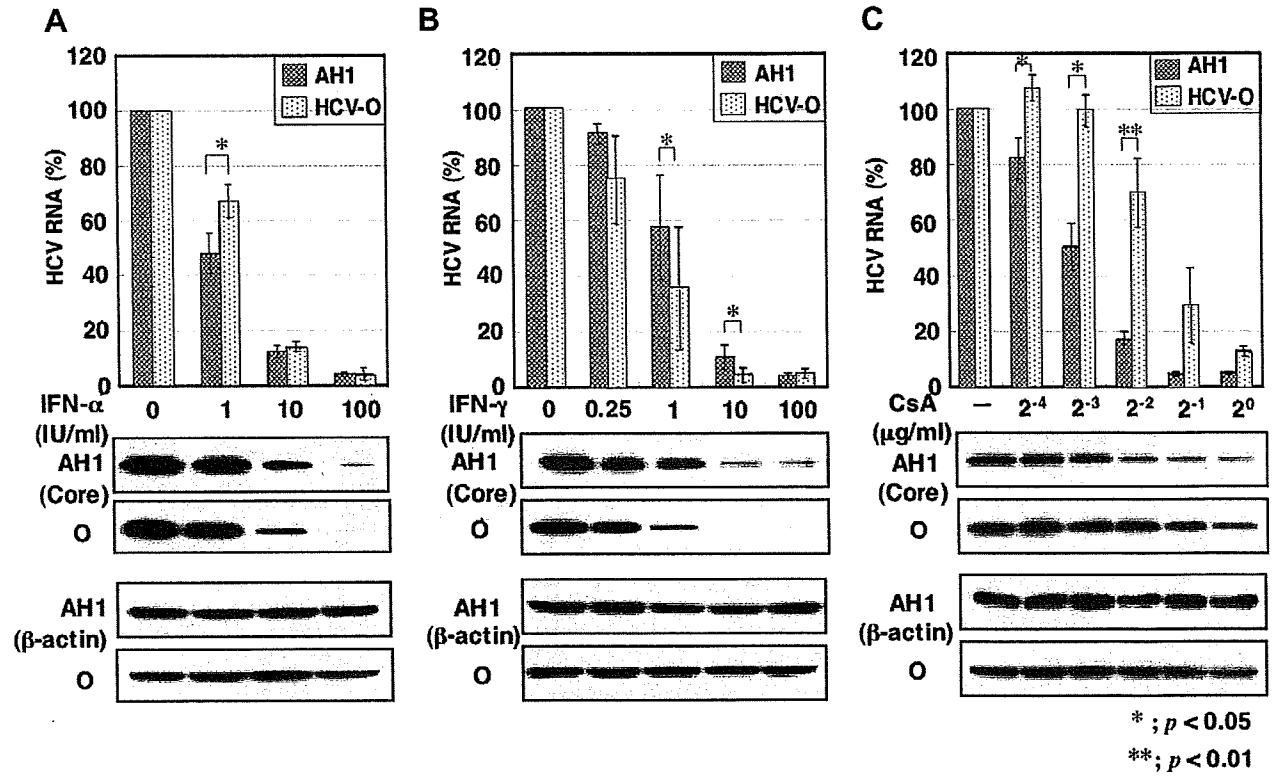

Fig. 3. The diverse effects of anti-HCV reagents on AH1 and HCV-O RNA replications. AH1 and O cells were treated with anti-HCV reagents for 72 h, and then extracted total RNAs and cell lysates were subjected to RT-qPCR for HCV 5′ UTR (each upper panel) and Western blot analysis for the core protein (each lower panel), respectively. (A) Effect of IFN-α. (B) Effect of IFN-γ. (C) Effect of CsA (Sigma).

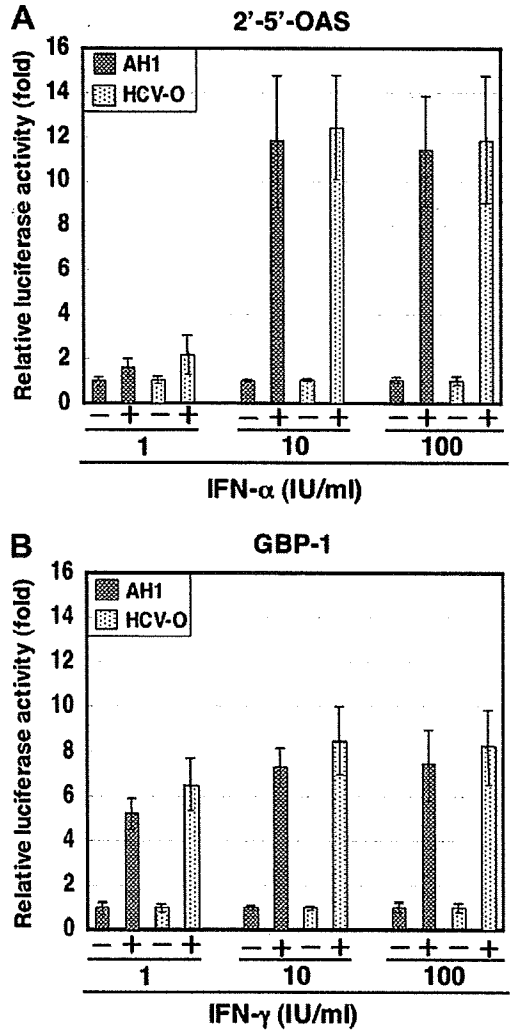

Fig. 4. Dual-luciferase reporter assay of IFN-α or IFN-γ-inducible gene promoter. AH1 and O cells were treated for 6 h with IFN-α or IFN-γ before the reporter assay. (A) 2′–5′-OAS gene promoter. (B) GBP-1 gene promoter.

with acute hepatitis C, and found diverse anti-HCV effects of IFN-γ and CsA between AH1 and HCV-O strains.

The levels of HCV replicon RNA and genome-length HCV RNA in sAH1 and AH1 cells were assigned to 3×10^7 and 2×10^7 copies/μg total RNA, respectively. These values are similar to those obtained from previously established HCV RNA replication systems [5]. Since known adaptive mutations (P1115L and V1897A) and additional conserved mutations (L1262S) were detected in the developed sAH1 replicon, these mutations may contribute to enhanced levels of RNA replication. The expression levels of genome-length HCV RNA and proteins observed in the present study suggest that genome-length HCV RNA replication efficiently occurs in AH1 cells, and that this RNA replication system is useful for comparison with already developed genome-length HCV RNA replication systems with HCV-N [7], Con-1 [8,9], or HCV-O [10] strains.

In the comparative analysis of genome-length HCV RNA replication systems with AH1 and HCV-O strains, we found that IFN-γ and CsA showed different anti-HCV profiles between AH1 and HCV-O strains. Regarding IFN-γ, RNA replication of the AH1 strain (EC_{50} = 1.9 IU/ml) was less sensitive than that of the HCV-O strain (EC_{50} = 0.3 IU/ml). Windisch et al. [18] have previously reported that RNA replication in an HCV replicon system using HuH-6 hepatoma cells is highly resistant (EC_{50} was more than 100 IU/ml) to IFN-γ, and that its resistant phenotype is not due to a general defect in the IFN-γ signaling pathway. In that study, they speculated that some mutations within a critical effector gene in HuH-6 cells might account for the inability of the cells to reduce the number of replicon RNAs in response to IFN-γ. Although such a possibility is not completely excluded, the diverse effects of IFN-γ observed in the present study were likely due to the difference in viral strains because RNA replication of the AH1 strain is still sensitive to IFN-γ. To clarify this point, development of an additional HCV RNA replication system such as an OR6 assay system with more quantitative reporter genes [10] is needed.

Regarding CsA, RNA replication of the AH1 strain (EC_{50} = 0.13 μg/ml) showed more sensitivity than that of the HCV-O strain (EC_{50} = 0.35 μg/ml). Ishii et al. [17] have previously reported that RNA replication of the JFH1 strain (genotype 2a) is less sensitive to CsA than genotype 1b strains, including the HCV-O strain. In that study, they concluded that the difference in sensitivity of JFH1 and genotype 1b strains to CsA could be attributed to characteristic differences in the HCV strains, not to the parent cell strain. In addition, sensitivity to CsA was almost the same among genotype 1b strains in that study. Therefore, we estimate that the AH1 strain is more sensitive to CsA than these genotype 1b strains examined to date. Further analysis will be necessary to clarify the mechanism underlying differences in sensitivity to CsA among genotype 1b strains.

In conclusion, an HCV RNA replication system with the AH1 strain would be useful for comparison with other strain-derived systems in various HCV studies, including analysis of the effects of anti-HCV reagents.

Acknowledgments

We thank T. Nakamura for technical assistance. We also thank A. Takamizawa and M. Kohara for the anti-NS3, NS4A, NS5A, and NS5B antibodies. This work was supported by grants-in-aid for a third-term comprehensive 10-year strategy for cancer control, and for research on hepatitis from the Ministry of Health, Labor, and Welfare of Japan.

Appendix A. Supplementary data

Supplementary data associated with this article can be found, in the online version, at doi:10.1016/j.bbrc.2008.04.005.

References

[1] D.L. Thomas, Hepatitis C epidemiology, Curr. Top. Microbiol. Immunol. 242 (2000) 25–41.
[2] N. Kato, M. Hijikata, Y. Ootsuyama, M. Nakagawa, S. Ohkoshi, T. Sugimurd, K. Sugimurd, Molecular cloning of the human hepatitis C virus genome from Japanese patients with non-A, non-B hepatitis, Proc. Natl. Acad. Sci. USA 87 (1990) 9524–9528.
[3] N. Kato, Molecular virology of hepatitis C virus, Acta Med. Okayama 55 (2001) 133–159.
[4] V. Lohmann, F. Korner, J. Koch, U. Herian, L. Theilmann, R. Bartenschlager, Replication of subgenomic hepatitis C virus RNAs in a hepatoma cell line, Science 285 (1999) 110–113.
[5] R. Bartenschlager, S. Sparacio, Hepatitis C virus molecular clones and their replication capacity in vivo and in cell culture, Virus Res. 127 (2007) 195–207.
[6] J.M. Pawlotsky, S. Chevaliez, J.G. McHutchison, The hepatitis C virus life cycle as a target for new antiviral therapies, Gastroenterology 132 (2007) 1979–1998.
[7] M. Ikeda, M. Yi, K. Li, S.M. Lemon, Selectable subgenomic and genome-length dicistronic RNAs derived from an infectious molecular clone of the HCV-N strain of hepatitis C virus replicate efficiently in cultured Huh7 cells, J. Virol. 76 (2002) 2997–3006.
[8] T. Pietschmann, V. Lohmann, A. Kaul, N. Krieger, G. Rinck, G. Rutter, D. Strand, R. Bartenschlager, Persistent and transient replication of full-length hepatitis C virus genomes in cell culture, J. Virol. 76 (2002) 4008–4021.
[9] K.J. Blight, J.A. McKeating, J. Marcotrigiano, C.M. Rice, Efficient replication of hepatitis C virus genotype 1a RNAs in cell culture, J. Virol. 77 (2003) 3181–3190.